https://doi.org/10.5194/acp-2020-1208
Preprint. Discussion started: 16 December 2020

Atmospheric Chemistry and Physics Discussions

The impact of Los Angeles basin pollution and stratospheric intrusions on the surrounding San Gabriel Mountains as seen by surface measurements, lidar, and numerical models

Fernando Chouza[1], Thierry Leblanc[1], Mark Brewer[1], Patrick Wang[1], Sabino Piazzolla[2], Gabriele Pfister[3], Rajesh Kumar[3], Carl Drews[3], Simone Tilmes[3], and Louisa Emmons[3]

[1]Jet Propulsion Laboratory, California Institute of Technology, Wrightwood, CA, USA
[2]Jet Propulsion Laboratory, California Institute of Technology, 4800 Oak Grove Drive, Pasadena, CA, USA
[3]National Center for Atmospheric Research (NCAR), Boulder, Colorado, USA

Correspondence: Fernando Chouza (keil@jpl.nasa.gov)

Abstract. In this work, the impact of Los Angeles basin pollution transport and stratospheric intrusions on the surface ozone levels observed in the San Gabriel Mountains is investigated based on a combination of surface and lidar measurements as well as WRF-Chem (Weather Research and Forecasting with Chemistry) and WACCM (Whole Atmosphere Community Climate Model) model runs. The number of days with observed surface ozone levels exceeding the National Ambient Air Quality Standards exhibit a clear seasonal pattern, with a maximum during summer, when models suggest a minimum influence of stratospheric intrusions and the largest impact from Los Angeles basin pollution transport. Additionally, measured and modeled surface ozone and PM10 were analyzed as a function of season, time of the day and wind direction. Measurements and models are in good qualitative agreement, with maximum surface ozone observed for south-west and west winds. For the prevailing summer wind direction, slightly south of the ozone maximum and corresponding to south south-west winds, lower ozone levels were observed. Back-trajectories suggest that this is associated with transport from the central Los Angeles basin, where titration limits the amount of surface ozone. A quantitative comparison of the lidar profiles with WRF-Chem and WACCM models revealed good agreement near the surface, with models showing an increasing positive bias as function of altitude, reaching 75% at 15 km above sea level. Finally, three selected case studies covering the different mechanisms affecting the near-surface ozone concentration over the San Gabriel mountains, namely stratospheric intrusions and pollution transport, are analyzed based on surface and ozone lidar measurements, as well as co-located ceilometer measurements and models.

1 Introduction

A high concentration of near-surface ozone poses a hazard to human health (WHO, 2003), animals, and vegetation (Mauzerall and Wang, 2001). Although consistent efforts regulating the emissions of ozone precursors in the Los Angeles (LA) basin region have led to a considerable reduction in the near-surface ozone levels (Pollack et al., 2013), the LA basin is still marked as a non-attainment area (EPA, 2020). For this reason, there has been an increased interest in understanding and modeling the different processes driving the near-surface ozone concentration with the aim to generate more effective air quality regu-

https://doi.org/10.5194/acp-2020-1208
Preprint. Discussion started: 16 December 2020

Atmospheric Chemistry and Physics Discussions

lation policies (Lin et al., 2017). Tropospheric ozone is mainly produced through photochemical processes involving carbon monoxide and volatile organic compounds in the presence of nitrogen oxides and sunlight (Monks et al., 2015). Additionally, stratospheric intrusions and elevated anthropogenic ozone plumes subject to long-range transport can also increase the tropo-
25 sphere ozone concentration and can, in some specific conditions, affect the near-surface air quality (e.g. Lin et al., 2012b; Knowland et al., 2017; Langford et al., 2018).

The Los Angeles basin shows one of the highest near-surface ozone concentration records in the United States. This is a consequence of several combining factors, including high precursor emissions associated with transportation and industry, high temperatures, and abundant sunlight, as well as meteorological conditions and surrounding mountains that limit the venting of
30 the accumulated smog (Lu and Turco, 1996; Langford et al., 2010).

While somewhat limited by topography and meteorological conditions, long-range transport of LA basin pollution has been identified as a source of high ozone events around the Mojave desert and other locations further away (Langford et al., 2010; VanCuren, 2015). Among the processes driving the transport of LA basin pollution, we can find low-level transport through several passes found between the mountains that surround the LA basin as well as transport over these mountains and injection
35 in the free troposphere caused by the up-slope flow mechanism, also refereed as the mountain chimney effect (Lu and Turco, 1996; Langford et al., 2010; De Wekker and Kossmann, 2015). While models and short-term measurements have been typically used to study these transport processes, no consistent long-term measurements have been conducted to quantify the frequency of these processes and investigate to which extent limited resolution models used for air quality forecasting reproduce them.

Additionally, many mountain-top monitoring stations have been typically assumed to sample free troposphere air and have
40 been used as part of a general effort to investigate long-term trends in background trace gas mixing ratios. While this assumption might be true in some stations or during particular periods, an assessment of the impact of local anthropogenic pollution sources is crucial to determine how well and during which periods this assumption of free troposphere sampling can be considered accurate (Lee et al., 2015; Tsamalis et al., 2014).

In this work, surface measurements conducted at the Jet Propulsion Laboratory Table Mountain Facility (JPL TMF) in the
45 San Gabriel Mountains (Southern California) for the last eight years and lidar measurements conducted between May 2019 and September 2020 are used to investigate the impact of LA basin pollution on the near-surface measurements carried at this mountain-top site. During the period under study, a few stratospheric intrusion events were recorded. Their influence on near-surface ozone is also briefly presented and discussed. Supporting Weather Research and Forecasting model coupled with Chemistry (WRF-Chem) and Whole Atmosphere Community Climate Model (WACCM) forecasts produced daily by the
50 Atmospheric Chemistry Observations and Modeling (ACOM) laboratory at the National Center for Atmospheric Research Atmospheric (NCAR) are also presented and evaluated to investigate how well current regional and global models can reproduce these observations considering the complex nature of the surrounding terrain.

The paper is organized as follows. Section 2 provides a general overview of the main characteristics of the LA basin region and the datasets used in this paper, including a description of the ozone lidar and ceilometer, surface instruments deployed at
55 JPL TMF, and the main setup characteristics of the WRF-Chem and WACCM models provided by NCAR ACOM. Section 3 presents an evaluation of the WRF-Chem forecast over JPL TMF based on ground and vertical profile measurements conducted

https://doi.org/10.5194/acp-2020-1208
Preprint. Discussion started: 16 December 2020

Atmospheric Chemistry and Physics Discussions

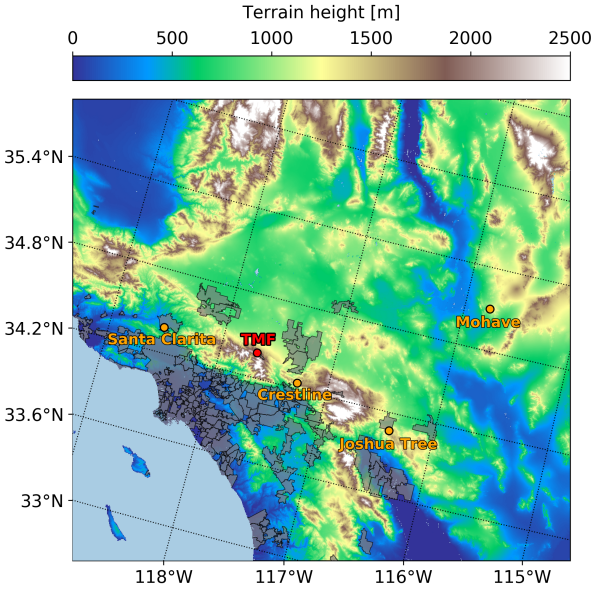

Figure 1. Terrain elevation of the LA basin and Mojave desert area. Urban regions are marked in grey. The location of TMF is marked in red, other surface ozone monitoring stations relevant for this study are marked in orange.

between May 2019 and September 2020 at TMF (the period during which the model data is available). In section 4, three case studies depicting the main mechanisms driving high surface ozone events at JPL TMF are discussed. Finally, a summary of the key findings of this paper is presented in Section 5.

2 Datasets and methods

2.1 Site description and data coverage

JPL Table Mountain Facility (34.38° N; 117.68° W, 2285 m a.s.l.) is located in the San Gabriel mountains (Fig. 1), north of the LA basin and 6 km north-west from Wrightwood, the closest town. The site host numerous instruments for air composition monitoring, including lidars and surface instruments (Table 1). Despite the high elevation, Chen et al. (2011) reported several days with signatures of anthropogenic pollution between late spring and early summer. Although these measurements already provide evidence of the LA basin impact at TMF, measurements based on the differential optical absorption spectroscopy (DOAS) have a limited capability to resolve the vertical extent of these anthropogenic layers. Similar results have been reported by Gorham et al. (2010) at Mt. Wilson (34.22° N; 118.06° W, 1742 m a.s.l.), another high elevation site located in the San Gabriel mountains. In that case, ground-based measurements of CO and non-methane hydrocarbons showed repeated signatures of LA basin pollution transport, with a peak occurrence during summer months.

https://doi.org/10.5194/acp-2020-1208
Preprint. Discussion started: 16 December 2020

Atmospheric Chemistry and Physics Discussions

Table 1. Datasets used in this work together with the period under study, temporal resolution and variables analyzed. Except for the two models, all the instruments are located at JPL TMF.

Dataset	Period	Temporal resolution	Variables used in this study
TMTOL	May 2019 - September 2020	1 hour	O_3 profile (0.1 to $\sim$15 km a.g.l)
CL51	May 2019 - September 2020	$\sim$15 seconds	Attenuated backscatter and boundary layer height
Thermo Fisher 49i	Juanuary 2012 - September 2020	1 minute	Surface O_3
Met One Model 212	May 2019 - September 2020	1 minute	Particle counts (0.3 µm-10 µm)
TMF Met station	May 2019 - September 2020	1 minute	Surface temperature, humidity, pressure and wind
ACOM WRF-Chem	May 2019 - September 2020	1 hour	O_3, anthropogenic CO, boundary layer height and wind
ACOM WACCM	May 2019 - September 2020	6 hours	Stratospheric ozone

2.2 Table Mountain tropospheric ozone lidar (TMTOL)

TMTOL is an ozone differential absorption lidar (DIAL) that has been under operation at JPL TMF since 1991. Under its original configuration, the system was able to alternate between ozone and aerosol measurements (McDermid et al., 1991). In 1999, the system was redesigned to provide routine measurements of tropospheric ozone in the middle and upper troposphere for the Network for the Detection of Atmospheric Composition Change (NDACC) (McDermid et al., 2002). This modification included the removal of the aerosol measurement capabilities, a larger telescope, and a receiver based on interference filters in place of the previous spectrometer-based one.

In 2018, TMTOL was fully automated and a new channel covering the range between 100 m a.g.l and 1000 m a.g.l was added to the system (Chouza et al., 2019). These two modifications greatly improved the capabilities of the system for air quality and transport studies in the PBL. Long runs of multiple hours or days can be routinely performed without over-stressing the operators, and the retrieved profile extends downwards into the PBL, in contrast to the former setup that allowed only measurements down to 1000 m a.g.l.. In addition to the validation with tethered balloons reported in Chouza et al. (2019), routine validations of this new very-near-range receiver have been conducted with an UAV-borne ozonesonde that provides ozone profiles between the ground and 120 m a.g.l.. The overlap of 20 m between the UAV measurements and TMTOL allows us to verify that the lidar measurement is not biased due to changes in the receiver overlap function. The results of these tests (36 in total) are summarized in Fig. 2. As can be seen, the difference between the first valid TMTOL retrieval and the UAV measurements has been generally under 10%, which is in agreement with previous TMTOL validation studies (Leblanc et al., 2018) and indicate good stability of the very-near-range receiver performance.

2.3 Vaisala CL51 ceilometer

Among the atmospheric remote sensing instruments at TMF, a Vaisala CL51 has been operated almost uninterruptedly since 2015. This instrument, located approximately 30 m west from TMTOL, provides valuable co-located qualitative information

https://doi.org/10.5194/acp-2020-1208
Preprint. Discussion started: 16 December 2020

Atmospheric Chemistry and Physics Discussions

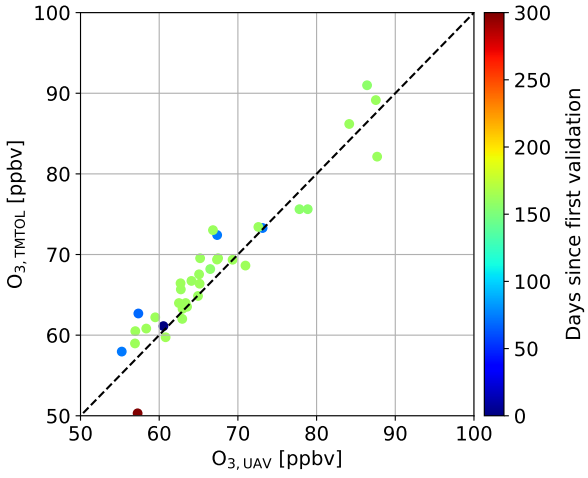

Figure 2. Comparison between the UAV-borne ozonesonde measurements and the corresponding TMTOL retrieval at 100-120 m a.g.l.. The scatter plot color indicates the number of days since the first UAV validation experiment (1 May 2019).

regarding the near-surface aerosol layers as well as planetary boundary layer (PBL) height measurements (Wiegner et al., 2014). In this study, the PBL height derivation is obtained from the proprietary Vaisala algorithms included in the original ceilometer software. While the details of this algorithms are not available to the users, a general description can be found in Münkel and Roininen (2010).

2.4 Surface measurements

In addition to TMTOL and the ceilometer, a set of in-situ measurement instruments that provide near-surface measurements of ozone, particulate matter, and meteorological variables are currently deployed at TMF. In the case of surface ozone, measurements are collected by a Thermo Scientific Model 49i Ozone Analyzer that has been operated at TMF since 2013 with a brief interruption in 2016 due to problems with the instrument. The surface ozone photometer inlet is located at about 2 m a.g.l. on the north side wall of TMTOL building. Particulate matter measurements have been carried out since 2015 by a Met One Model 212, covering particle size from 0.3 µm to 10 µm. This instrument is located about 60 m south from TMTOL at an altitude of about 2 m a.g.l.. The PM10 values reported in this work have been obtained from the particle counter following Brattich et al. (2020). Finally, meteorological variables including temperature, humidity, and wind speed have been collected with the current setup since 2005 with only a few short interruptions driven by failures in the data acquisition system. The meteorological mast where the instruments are attached is approximately 30 m west from TMTOL. The wind speed and direction sensor is located at 10 m a.g.l., while the rest of the sensors are at 2 m a.g.l..

https://doi.org/10.5194/acp-2020-1208
Preprint. Discussion started: 16 December 2020

Atmospheric Chemistry and Physics Discussions

2.5 ACOM WRF-Chem forecast

The WRF-Chem air quality predictions are produced daily at NCAR using version 3.9.1 of the WRF-Chem model (Fast et al., 2006; Grell et al., 2005; Powers et al., 2017). The model domain is defined on a lambert conformal project with a horizontal grid spacing of 12 x 12 km^2. The model domain covers the contiguous United States (CONUS) with 390 and 230 grids points in longitudinal and latitudinal directions, respectively. The vertical grid in the model is composed of 43 levels stretching from the surface to 50 hPa. A detailed description (chemical and physical parameterization, emissions, driving meteorological and chemical fields) of the forecasting system configuration can be found at https://www.acom.ucar.edu/firex-aq/tracers.shtml and only details relevant to this study are summarized here.

Tropospheric ozone photochemistry is represented using the Model for Ozone and Related Tracers-4 (MOZART-4) chemical mechanism (Emmons et al., 2010). MOZART-4 contains 83 species that participate in 157 gas-phase reactions and 38 photolysis reactions. The model does not include stratospheric chemistry and lateral boundary conditions control the background as well as upper atmospheric concentrations. In addition, six carbon monoxide (CO) source tracers are included in the model to keep track of CO emitted from anthropogenic and biomass burning emission sources located inside the domain, photochemical production of CO from non-methane volatile organic compounds (NMVOCs) emitted within the domain, and background CO flowing into the domain produced by all non-CONUS sources including non-CONUS fires. CO tracers are subjected to the same physical and chemical losses (reaction with OH and deposition) as the standard CO species is but do not affect any atmospheric processes in the model.

The U.S. EPA National Emissions Inventory (NEI) 2014 is used to represent monthly varying anthropogenic emissions of trace gases and aerosols. No adjustments were made to the emissions due to COVID-19 related restrictions. Fire Inventory from NCAR (FINN) version 1 (Wiedinmyer et al., 2011) provides near-real-time (NRT) biomass burning emissions to the model, which are distributed vertically online within the model using a plume rise parameterization (Freitas et al., 2007). NRT FINN emissions are available with a latency of 1 day and are assumed to persist over the forecast cycle. The meteorological initial and boundary conditions are based on the 00 UTC cycle of the Global Forecast System (GFS) produced daily by the National Oceanic and Atmospheric Administration (NOAA). The chemical boundary conditions are based on the WACCM forecasts produced daily by NCAR (see Sec. 2.6 for WACCM details). The initial conditions for chemical fields are based on previous day's forecast. Hourly model output is saved for analysis. A two-day model forecast starts at 2 am MT every day and finishes in about 2 hours. Selected model output including concentrations of ozone, PM2.5, key precursor species, meteorological variables, and NRT observations of surface ozone and PM2.5 are displayed at https://www.acom.ucar.edu/firex-aq/forecast.shtml for dissemination to the public.

2.6 ACOM WACCM

The Whole Atmosphere Community Climate Model Version 6 (WACCM6) is one of the atmospheric components of the Community Earth System Model (CESM2) (Gettelman et al., 2019). WACCM6 is a fully coupled global Earth System model that extends from the Earth's surface towards the lower thermosphere ($\sim$ 150 km altitude). The chemistry scheme is the

https://doi.org/10.5194/acp-2020-1208
Preprint. Discussion started: 16 December 2020

Atmospheric Chemistry and Physics Discussions

MOZART Troposphere Stratosphere Mesosphere and Low Thermosphere Version 1 (TSMLT1) chemical mechanism (Emmons et al., 2020). The aerosol scheme is the Modal Aerosol Model (MAM4), including a volatility basis set (VBS) description of secondary organic aerosols (Tilmes et al., 2019).

For this study, it uses a horizontal resolution of 0.9° latitude x 1.2° longitude. The specified dynamics version used here adopts the levels of GEOS5 below 50 km and has a total of 88 vertical levels reaching to the model top. The simulation used in this study uses observed sea-surface temperatures and sea-ice conditions for present day that is coupled to the community land model Version 5 (CLM5). The atmospheric winds, temperature, and surface fluxes are nudged below 50 km towards NASA GMAO GEOS5.12 meteorological analysis with a Newtonian relaxation of 50 hours. Daily fire emissions are based on FINNv1. Anthropogenic emissions are from the CAMS Version 3 (Copernicus Atmosphere Monitoring Service) inventory. Biogenic emissions are derived using the Model of Emissions of Gases and Aerosols from Nature version 2.1 incorporated in the CLM (Guenther et al., 2012). A stratospheric ozone tracer is included in this configuration, which is set equal to ozone in the stratosphere and destroyed in the troposphere at the same rate as the model ozone (photochemical destruction and dry deposition).

This model version has been also used to provide a daily 10-day forecast since 2018, using GEOS5 meteorological forecast fields plots and output files that are available at https://www2.acom.ucar.edu/acresp/forecasts-and-near-real-time-nrt-products.

3 WRF-Chem evaluation

3.1 Surface ozone and PM10

While Granados-Muñoz and Leblanc (2016) already provided an overview of the surface ozone characteristics at TMF for the period 2013-2015, additional analysis as well as supporting model information are expected to help to better characterize the impact of the LA basin pollution at TMF. Figure 3a shows a histogram of ozone exceedances based on the surface ozone measurements conducted at TMF from January 2012 to September 2020. Due to a malfunction of the TMF surface ozone analyzer, measurements from 2016 are excluded from this study. While variable from year to year, the number of days with ozone levels exceeding the EPA regulations follow a clear progression over the months, with almost no exceedances during winter and a large number of exceedances during summer. A remarkably low number of exceedances were observed in 2019, which is likely associated with below-average temperatures (not shown). Since the local production of ozone precursors is very limited in the San Gabriel mountains, the origin of these exceedances is likely related to direct transport from the LA basin region as previously reported in the case study presented in Langford et al. (2010). Together with anthropogenic pollution transport, stratospheric intrusions have also been pointed as the cause of high surface ozone events in the region (Lin et al., 2012a). Since no isotope-based stratospheric tracer measurements (Stohl et al., 2000) are available at TMF, the surface impact of stratospheric intrusions is hard to quantify. Nevertheless, Fig. 3b provides an overview of the stratospheric tracer reported by WACCM at 2700 m a.g.l. since May 2019 over TMF. This figure shows a clear pattern in the number of deep intrusions, with a maximum during winter and early spring, and a minimum during summer and early fall. This seasonality is in agreement with previous studies in the region (Granados-Muñoz and Leblanc, 2016). Together with the box plot, the value of the stratospheric

https://doi.org/10.5194/acp-2020-1208
Preprint. Discussion started: 16 December 2020


Atmospheric Chemistry and Physics Discussions

ozone contribution reported by WACCM during exceedance days is also shown. In most cases, the WACCM stratospheric ozone levels during exceedance days fall within 1.5 times the inter-quartile range (IQR), which suggests that it plays a limited role in most ozone exceedance cases. Similarly, relative humidity and temperature are also presented, as intrusions are typically associated with cold fronts and dry air. While this analysis does not rule out stratospheric intrusions as the cause of some of the exceedances, their overall impact appears to be limited according to the WACCM model.

Since LA basin pollution transport seems the most likely cause for the large number of exceedances observed during the March-October period, an analysis of the ozone and PM10 levels as a function of local time and wind direction is presented in Fig. 4 for the period between summer 2019 and summer 2020. As supporting information, ozone, PM10, and anthropogenic CO provided by the ACOM WRF-Chem forecast is also included for the same period. The first and fourth rows, which present the number of values observed and forecasted for each time of the day and wind direction, reveal prevailing winds almost exclusively from the south south-west (SSW) during summer and spring with very little temporal variability. During fall and winter, a second prevailing wind direction can be seen coming from the east north-east (ENE). WRF-Chem shows a very similar pattern, with fewer SSW points during winter and slight changes in the prevailing wind directions.

In the case of the ozone measurements and forecast (second and fifth rows), the largest mean values appear in the summer early night extending in some cases into the next day. In the case of WRF-Chem, the peak in the mean ozone has a similar amplitude but is approximately 3 hours earlier than observed and minimum ozone values during morning time are significantly lower (about 10 ppbv) than the measured ones, which leads to an overestimation of the ozone diurnal cycle amplitude by the model. The ozone mean is observed to peak for south-west and west winds, slightly north from the prevailing wind direction. For the prevailing wind direction, the observed ozone levels during summer 2019 and 2020 show surprisingly low values, about 10 ppbv below the values observed for west winds. In the case of the forecast, this feature is well reproduced for summer 2019, while for summer 2020, this feature is less pronounced (note that neither WACCM nor WRF-Chem have emissions adjusted for COVID-related restrictions). To understand the origin of this difference, HYSPLIT/PySplit (Stein et al., 2016; Warner, 2018) back-trajectories for summer 2019 (Fig. 5) and summer 2020 and (Fig. 6) were calculated starting at 2:00 UTC (peak of surface ozone at TMF) for 4 hours, which corresponds to the typical time difference with respect to the ozone maximum in the central LA area (Granados-Muñoz and Leblanc, 2016). These trajectories were separated into two groups, one corresponds to the days where the wind direction was between 250 and 300 degrees (Figs. 5 and 6, first column) and a second group, where the wind direction was between 210 and 240 degrees (Figs. 5 and 6, second column). For both groups, the trajectories were started at 10 m above TMF. Additionally, the mean modeled surface ozone (Figs. 5a,b and 6a,b), NO_2 (Figs. 5c,d and 6c,d) and PM10 (Figs. 5e,f and 6e,f) at the time of the end of the back-trajectories (4 hours before the start, peak ozone in central LA) were calculated for these two groups. The surface ozone pattern, as reported in Lu and Turco (1996), is similar for these two cases, with high ozone in the Santa Clarita/San Fernando Valley area and the eastern LA basin and relatively low surface ozone in the central LA area. This can be attributed to enhanced near-surface titration associated with high surface NO_2 levels (Figs. 5c,d and 6c,d). The trajectories corresponding to the prevailing winds end over this high surface NO_2 region, which likely explains the difference with respect to the west wind back-trajectories that mainly end in the San Fernando Valley area. During fall and spring similar patterns are observed, but with an overall lower ozone concentration. As in the summer case,

https://doi.org/10.5194/acp-2020-1208
Preprint. Discussion started: 16 December 2020

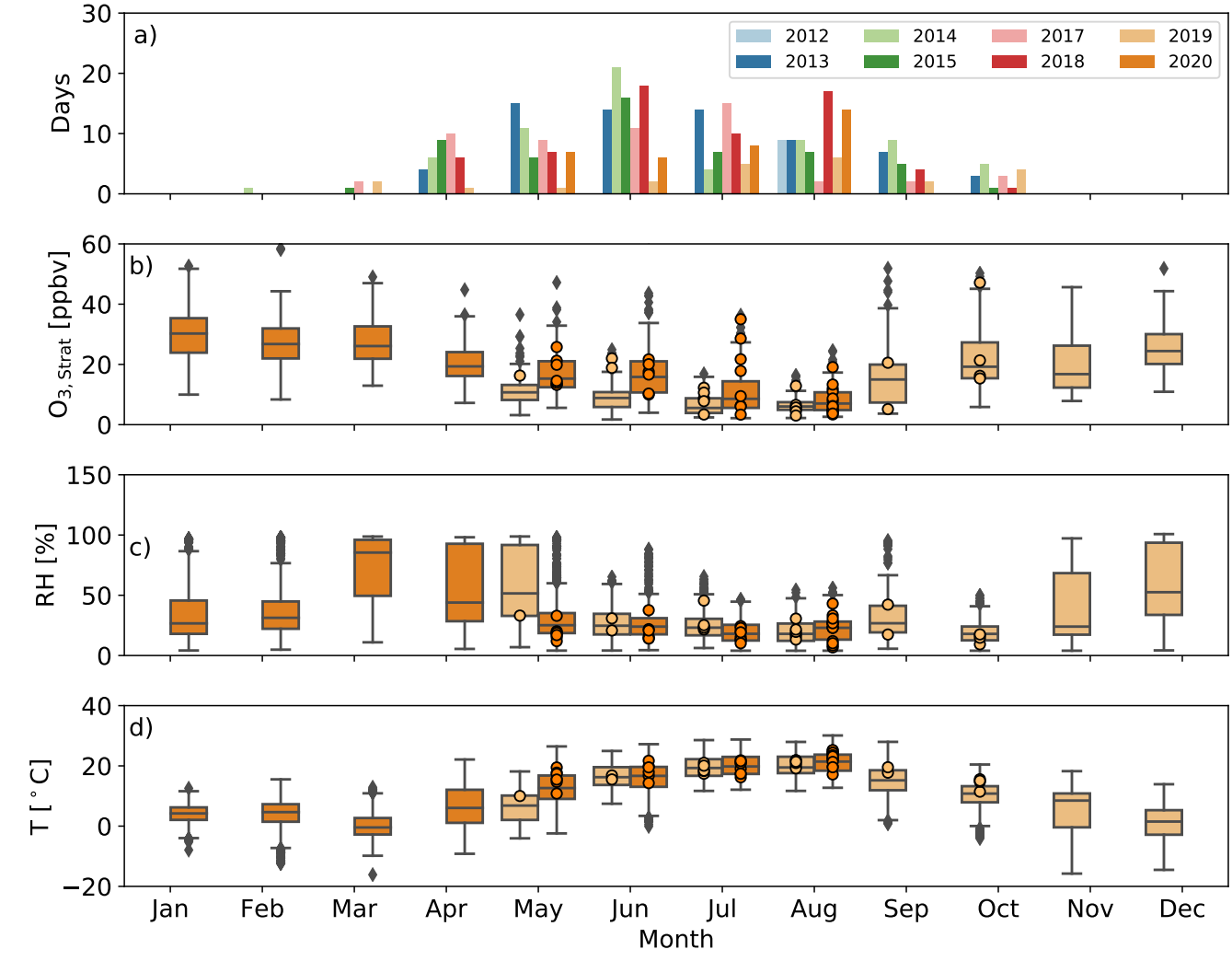

Figure 3. (a) Number of days exceeding the EPA maximum ozone regulations (>70 ppbv 8h MDA) as function of month and year between 2012 and June 2020. (b) WACCM forecast of the stratospheric ozone at 2700 m a.s.l. as function of month and year between May 2019 and June 2020 presented as a box plot. The WACCM stratospheric ozone values for the exceedance days are shown as a scatter plot. (c,d) Surface relative humidity and temperature for the same period presented in (b). Relative humidity and temperature measurements during the exceedance days are shown as scatter plots.

the forecasted nighttime ozone concentration is lower than the observed one. During winter, forecasted and observed ozone exhibits the largest homogeneity among seasons, with very little dependence with time or wind direction.

During summer 2019, PM10 observations and forecast (third and sixth rows) exhibited a pattern very similar to the one observed for ozone, with a diurnal cycle peaking in the afternoon for west and north-west winds. For the prevailing SSW

https://doi.org/10.5194/acp-2020-1208
Preprint. Discussion started: 16 December 2020

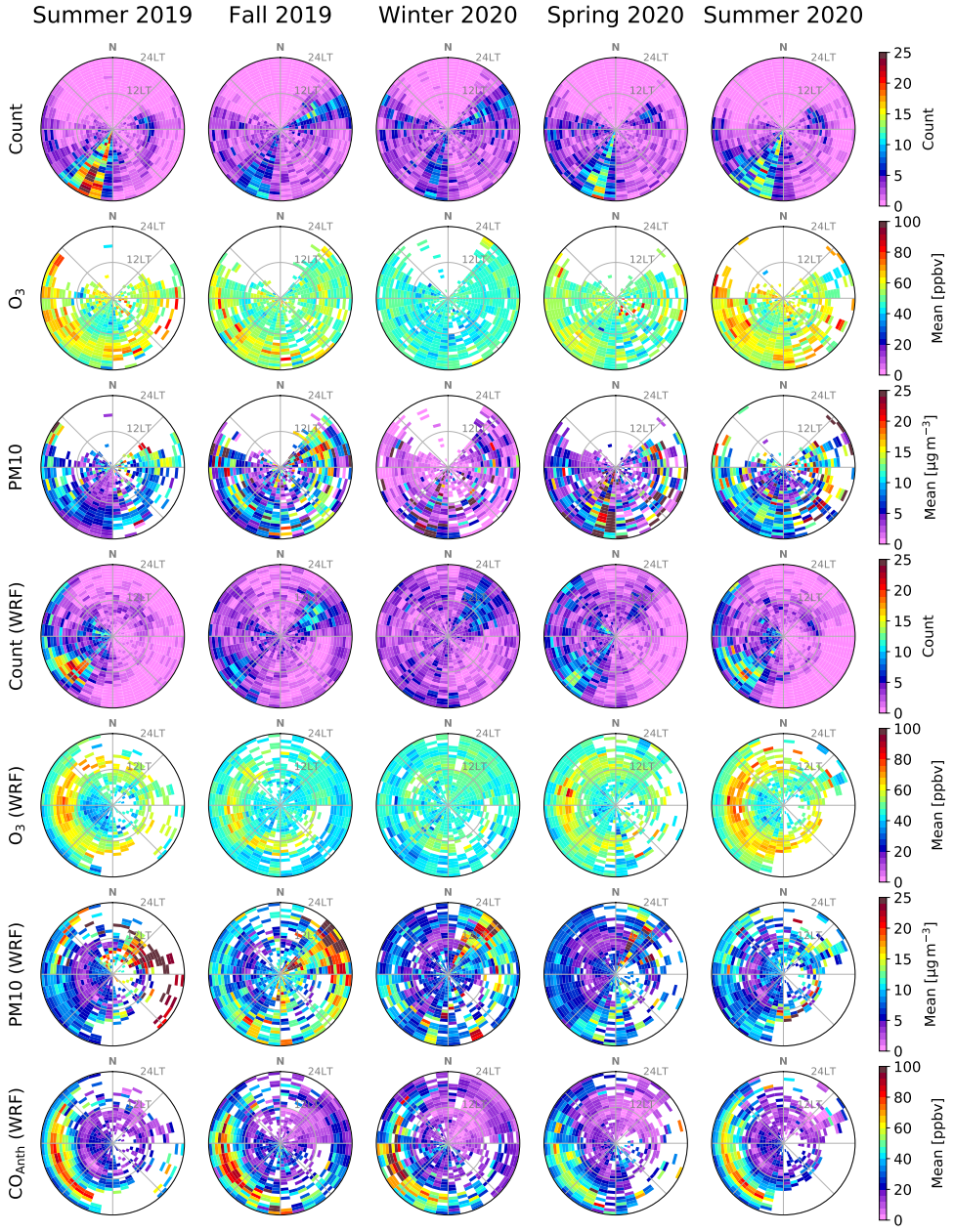

Figure 4. Overview of the number of surface measurements (first row), mean ozone (second row) and mean PM10 (third row) at TMF as function of the time of the day (radial direction, local time), wind direction (angular) and season (columns) for the period comprehended between June 2019 and September 2020. The corresponding values forecasted by WRF-Chem are presented in the fourth, fifth and sixth rows, with the addition of the anthropogenic CO contribution (last row).

https://doi.org/10.5194/acp-2020-1208
Preprint. Discussion started: 16 December 2020


Atmospheric Chemistry and Physics Discussions

winds, a minimum in the PM10 is observed and forecasted. A remarkable difference is nevertheless observed for ENE winds, where a second PM10 maximum in the afternoon can be distinguished, likely associated with dust transported from the Mojave desert. During fall and spring, and although there is still a qualitative agreement between measurements and forecast, the forecasted PM10 values are generally larger than the measured ones. The winter PM10 measurements show very little aerosol load, while WRF-Chem shows a pattern similar to spring and summer. In contrast to the observations and forecast presented for summer 2019 and the forecast for summer 2020, summer 2020 PM10 observations shows generally larger concentrations and no minimum associated with south south-west (SSW) winds. The explanation for this discrepancy is unknown, but might be associated with enhanced aerosol load product of extensive wildfires occurred during summer 2020.

Finally, the anthropogenic CO forecast (last row) provides a clear view of the LA transport process, with relatively low seasonal variability, a clear maximum in the late afternoon and south to south-west winds.

3.2 Vertical ozone profile

While surface measurement instruments like the 49i Ozone Analyzer and the particle counter provide almost continuous datasets (Sec. 3.1), vertical profiles, as obtained by lidars and balloons, are often required to understand the vertical extent, source, and potential for long-range transport of different types of high surface ozone events. In the case of TMF, this is especially true, as the surrounding mountainous terrain adds a layer of complexity to the transport processes and the interpretation of surface measurements.

The previous long-term study presented in Granados-Muñoz and Leblanc (2016) focused in the free troposphere, as the minimum TMTOL range was mainly limited to 1.3 km a.g.l., which left out of the study most of the PBL. The new very-near range channels, able to reach as low as 100 m a.g.l., have been operated and validated in a routine manner since their installation in mid-2018, allowing almost complete coverage of the PBL. Additionally, during the last two years, longer run periods of multiple days have been regularly conducted by TMTOL in order to capture forecasted SI and LA pollution transport events with the aim to understand the relative contribution of these to the observed exceedances at TMF and investigate to what extent the forecasting tools are able to reproduce them.

While validation of surface ozone and PM forecast is conducted as part of the ACOM WRF-Chem model runs on a routine basis, vertical evaluation is typically restricted to specific locations, as this type of measurement is not nearly as common as the surface ones. In addition to the multi-day runs focused on particular events, TMTOL has continued its regular operations consisting of one hour daily measurements during TROPOMI overpasses (typically around 1 pm local time) and 2-hour measurements 4 to 5 times per week during early nighttime. In this section, all the profiles retrieved from TMTOL since the beginning of the ACOM WRF-Chem forecast runs (May 2019) are used to evaluate the general performance of the model over TMF.

Due to the complex nature of the terrain surrounding TMF, an assessment of the impact of the terrain smoothing associated with the limited spatial resolution of WRF-Chem has to be made. Figure 7 presents an overview of the WRF-Chem terrain elevation in the LA basin area, together with two cross-sections showing the difference between the actual and WRF-Chem terrain elevations. The A-A' cross-section is selected to be parallel to the prevailing winds in the region, while the B-B' is

https://doi.org/10.5194/acp-2020-1208
Preprint. Discussion started: 16 December 2020

Atmospheric Chemistry and Physics Discussions

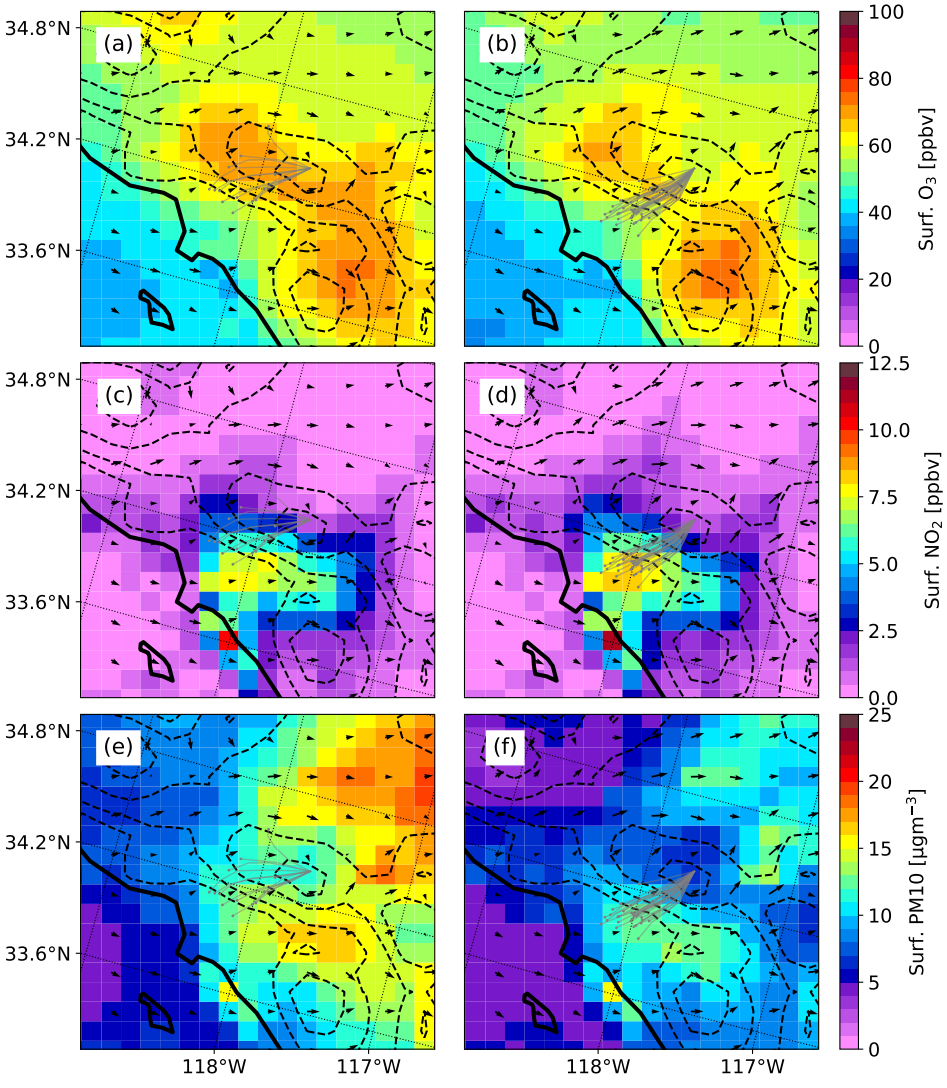

Figure 5. Back-trajectories (grey) started at TMF at 2:00 UTC and ended at 22:00 UTC (-1 day) are shown together with the corresponding mean modeled surface O_3 (a,b), NO_2 (c,d) and PM10 (e,f) at the time of the end of the trajectories for two TMF wind direction groups during summer 2019. (a,c,e) Trajectories started on days where the surface winds over TMF were between 250 and 300 degrees at 2:00 UTC. (b,d,f) Trajectories started on days where surface winds over TMF were between 210 and 240 degrees. 10-m winds are also shown (black arrows). Elevation contours are shown (dashed black) for 250, 500, 1000 and 1500 m a.s.l.

almost perpendicular to A-A' and provides a general view of the passes and mountains that affect the outflow of the LA basin pollution. Both cross-sections were selected to run over TMF.

https://doi.org/10.5194/acp-2020-1208
Preprint. Discussion started: 16 December 2020

Atmospheric Chemistry and Physics Discussions

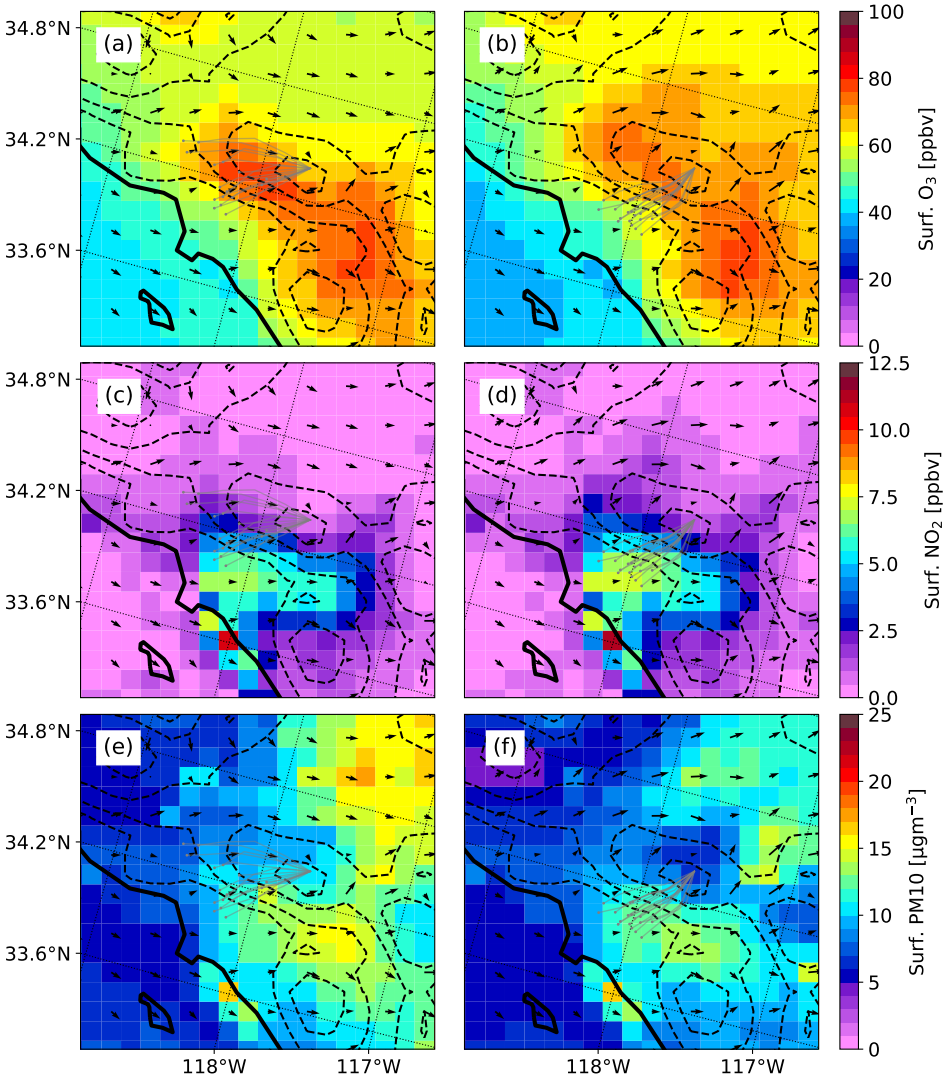

Figure 6. Same as Fig. 5, but for summer 2020.

Thanks to the relative smoothness of the mountains surrounding the LA basin, a fairly good agreement between the actual terrain and the model terrain can be seen along the two cross-sections. The difference at TMF is among the largest ones, with the actual elevation being about 2.3 km and the modeled one about 1.7 km. Since this difference is mainly restricted to the top of the mountain, the effect on the mountain venting process and the associated vertical ascent is expected to be small.

https://doi.org/10.5194/acp-2020-1208
Preprint. Discussion started: 16 December 2020

Atmospheric Chemistry and Physics Discussions

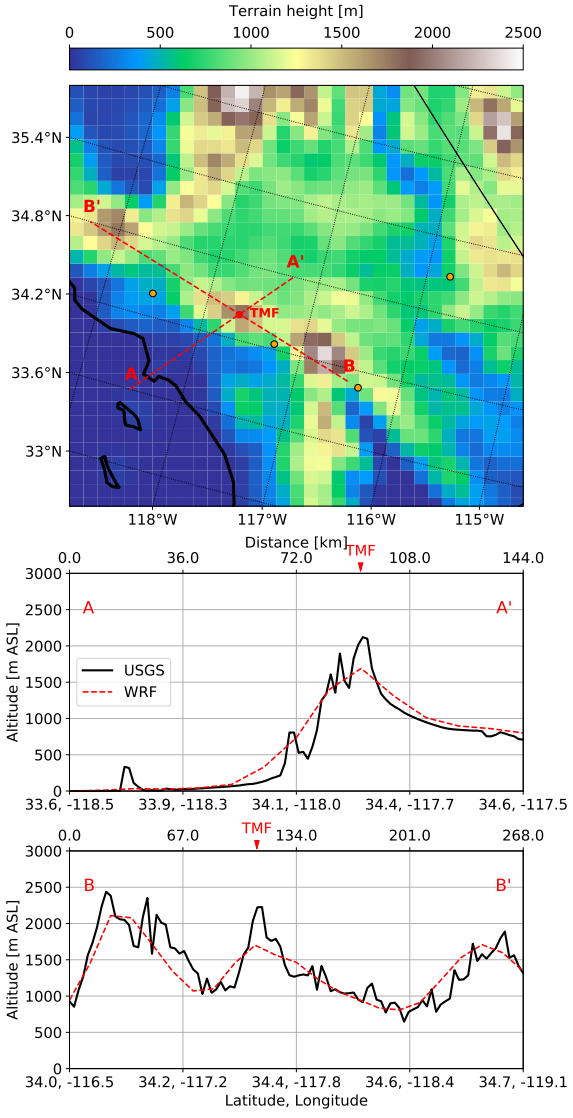

Figure 7. Overview of the terrain elevation used as part of the WRF-Chem simulation for the area under study. The TMF location, as well as the actual (solid, black) and WRF-Chem (dashed red) elevation profiles are shown two selected cross-sections used in this study.

Figure 8 presents an overview of the comparison between TMTOL and WRF-Chem for the same period analyzed in Sec. 3.1 (summer 2019 to summer 2020), with each row of the plot corresponding to one season. Additionally, the profiles are separated in nighttime and daytime to investigate the impact of the diurnal cycle in the model performance and the resolution change in the TMTOL retrieval. The first column of Fig. 8 shows the TMTOL profiles available for each season and time of the day (a total of 726 profiles), together with the corresponding mean profile. The second column shows the temporally closest WRF-Chem profile (excluding profiles corresponding to the model spin-up period) to each TMTOL profile shown in the first column,

https://doi.org/10.5194/acp-2020-1208
Preprint. Discussion started: 16 December 2020

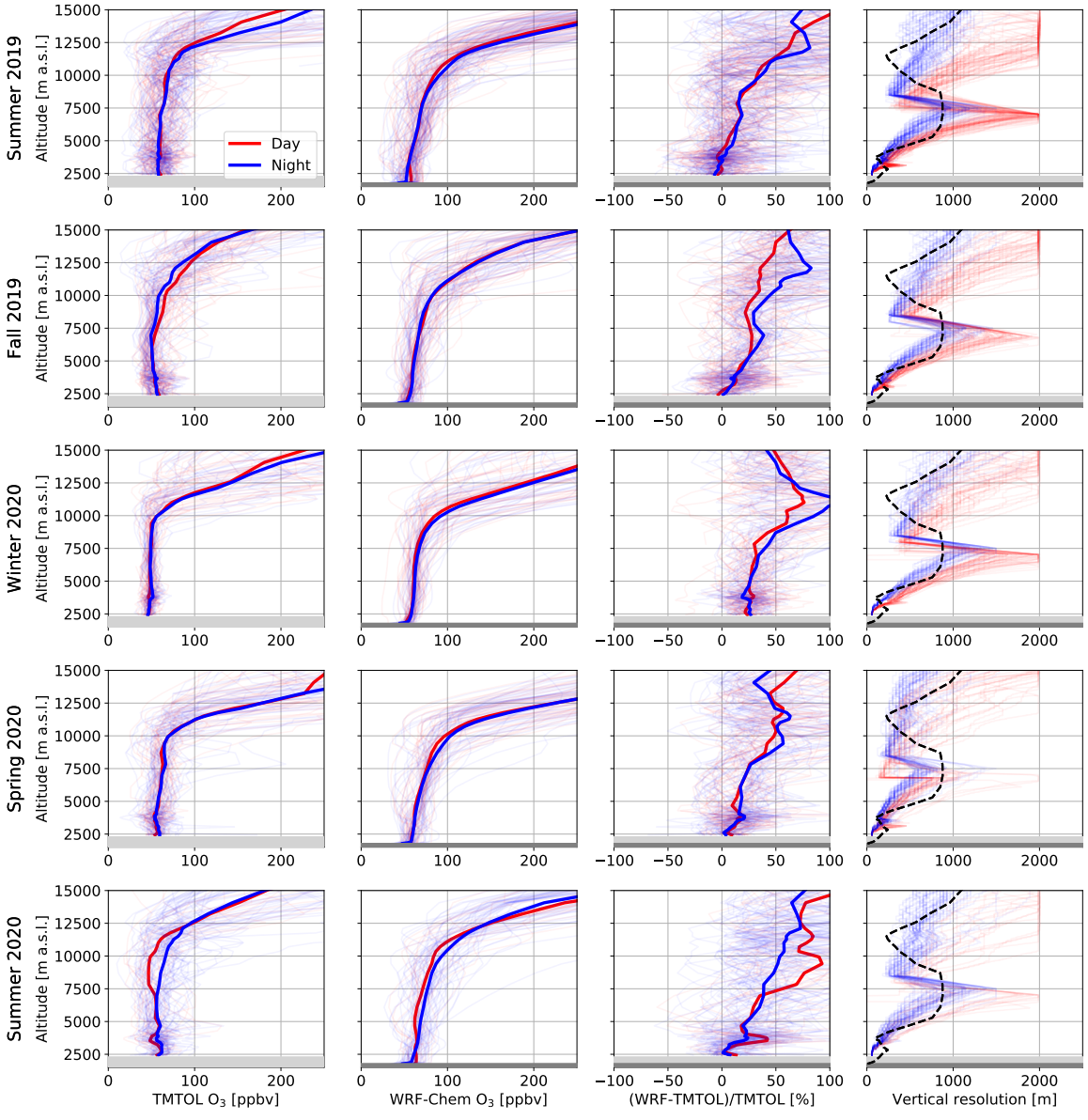

Figure 8. Relative difference (third column) between TMTOL (first column) and WRF-Chem (second column) ozone profiles for the period between summer 2019 and summer 2020 (rows). Individual profiles are shown (thin lines) together with the corresponding seasonal mean (thick lines) for daytime (red) and nighttime (blue) profiles. TMTOL retrieval vertical resolution (thin lines) as well as the model vertical grid (dashed black) are also shown for each season and time of the day (fourth column). Actual ground level and WRF-Chem surface level are shown as grey and dark grey shaded areas respectively.

https://doi.org/10.5194/acp-2020-1208
Preprint. Discussion started: 16 December 2020


Atmospheric Chemistry and Physics Discussions

as well as the mean of these profiles. The third column presents the relative difference between each individual TMTOL and corresponding WRF-Chem profile, as well as the mean of these differences. In order to perform this comparison, the TMTOL profiles are averaged over each level of the model grid. As supporting information, the vertical resolution for the TMTOL retrieval (Leblanc et al., 2016), is presented together with the WRF-Chem model vertical resolution in the fourth column. It is important to notice that the TMTOL vertical resolution is mainly controlled by the signal-to-noise ratio and the specified retrieval uncertainty. For a fixed uncertainty, the vertical resolution degrades as the amount of solar background increases. For this reason, the vertical resolution during daytime experiments is generally lower than during nighttime. Additionally, since TMTOL consists of different receivers looking at different altitude ranges, the vertical resolution changes as a function of altitude. This change in receivers can be seen as sharp changes in the vertical resolution at around 3 km and 7-8 km.

Overall, the WRF-Chem forecast shows an excess of ozone across the full range under analysis, independent of season and time of the day. This excess is limited to about 25% in the PBL, but increases almost monotonically with altitude reaching differences of up to 75% at 15 km. No clear difference in the model bias behavior was observed across the tropopause, typically found between 12 km a.s.l. (winter) and 16 km a.s.l. (summer). With respect to the seasonal trends, a good qualitative agreement between the model and TMTOL is observed, with an ozone increase in the UTLS (upper troposphere lower stratosphere) region, with lower and sharper transitions than during winter.

4 High surface ozone drivers at TMF

The previous section presented a general overview of the ozone and surface PM10 characteristics at TMF as well as an evaluation of the WRF-Chem capabilities to reproduce them. In this section, three case studies are presented to illustrate specific mechanisms by which the surface or near surface ozone concentration at TMF can be affected, and investigate the extent to which WRF-Chem is able to reproduce them.

4.1 3 July 2020: A deep stratospheric intrusion event

This case study, based on measurements conducted by TMTOL on 3 July 2020 between 4:50 and 17:50 UTC, illustrates the effect of a deep stratospheric intrusion on the surface ozone concentration at TMF. Since deep stratospheric intrusions typically occur during spring and not necessarily significantly affect the surface ozone concentration, the case study presented in this section represents a rarity in both ways. Additionally, and although WRF-Chem and WACCM forecasted enhanced ozone in the lower free troposphere associated with a SI, WRF-Chem did not forecast an effect on the surface ozone as it finally occurred, which illustrates the challenges associated with modeling the entrainment into the nocturnal surface layer and in complex terrain.

Figure 9a presents an overview of the forecasted WRF-Chem ozone, anthropogenic CO (grey-shaded contours), PBL height (dashed black), and WACCM stratospheric ozone contribution (hatched contours) for the period comprehended between 2 July 2020 12:00 UTC and 4 July 2020 0:00 UTC. The forecast, which motivated an extended TMTOL run, starts with moderate ozone enhancement in the PBL during 2 July with an associated increase of anthropogenic CO, suggesting transport from the

https://doi.org/10.5194/acp-2020-1208
Preprint. Discussion started: 16 December 2020


Atmospheric Chemistry and Physics Discussions

LA basin area. After the collapse of the PBL, a persistent layer of high ozone (about 70 ppbv) is visible between the ground and 3.5 km a.s.l., with a small drop around 3 July 6:00 UTC. Until that point, the forecast can be seen as a typical case of LA basin pollution transport, with ozone being injected into the free troposphere after the collapse of the PBL. Nevertheless, after 6:00 UTC, a second increase of the ozone in the lower troposphere is visible, which later extends into an ozone-rich stratospheric air tongue with ozone levels exceeding 70 ppbv. The stratospheric origin of this enhancement is supported by the co-located low relative humidity from WRF-Chem, as well as the stratospheric ozone tracer from WACCM, which shows a contribution of over 30 ppbv on 3 July between 4:00 and 13:00 UTC at about 2.5 km a.s.l.. After 13:00 UTC, and as the PBL starts to grow, the influence of the SI starts to decrease and a new transport wave of LA basin pollution takes over as the main ozone driver in the PBL.

While the models presented in Fig. 9a are in qualitative agreement with the TMTOL measurements (Fig. 9b), measurements show a shallower layer with a much stronger enhancement in the ozone levels below 3 km a.s.l. and a less defined stratospheric air tongue than the simulation. During the whole measurement period, the observed layer was characterized by ozone levels of over 100 ppbv (as opposed to the 70 ppbv forecasted by WRF-Chem) and low aerosol load levels (Fig. 9c). Another significant difference is related to the surface influence of the SI. Figure 9d presents a time series of forecasted and measured surface and 100 m a.g.l. ozone mixing ratio, as well as the measured relative humidity at TMF. While the WRF-Chem simulation forecasted an almost constant 50 ppbv surface ozone level, compatible with nighttime background conditions, the 49i Ozone Analyzer shows increasing ozone values after sunset, reaching 90 ppbv between 9:00 and 11:00 UTC. While looking at the 100 m a.g.l., no significant difference was observed between the first valid TMTOL data point (100 m a.g.l.) and the surface, while the WRF-Chem model showed a gradient of about 15 ppbv between surface and 100 m a.g.l..

In order to provide a broader context to this case study, the same variables shown in Fig. 9a for 3 July 6:00 UTC are presented in Fig. 10 for a constant altitude of 2.5 km a.s.l. around the LA basin area as well as for the two cross-sections defined in Fig. 7.

The constant altitude cross-section (Fig. 10a) shows a well defined high ozone filament south-west of TMF associated with high speed south winds and low humidity (not shown). Slightly north from TMF, a second plume of high ozone and anthropogenic CO (LA basin pollution) can be seen being displaced by this high ozone filament from stratospheric origin. The cross-sections presented in Figs. 10b and 10c provide an additional overview of the stratospheric tongue geometry as well as the stratospheric contribution forecasted by WACCM (hatched contours). The A-A' cross-section shows also very low ozone over the LA basin area, as usually found during nighttime and suggests that little or no impact of this SI was forecasted.

4.2 27-29 May 2020: A LA pollution transport event

Between 27 May and 28 May, two TMTOL extended runs were decided based on the WRF-Chem forecast of high surface ozone and anthropogenic CO levels (grey-shaded contours) associated with LA basin pollution transport (Fig. 11a). For the early part of 27 May (the late afternoon of 26 May if local time is considered), low levels of stratospheric influence were forecasted by WACCM (hatched contours), while during the late part of 27 May and beginning of 28 May, a common case of LA basin pollution transport was expected with no stratospheric influence below 6 km a.s.l.. In this latter case, simulated

https://doi.org/10.5194/acp-2020-1208
Preprint. Discussion started: 16 December 2020

Atmospheric Chemistry and Physics Discussions

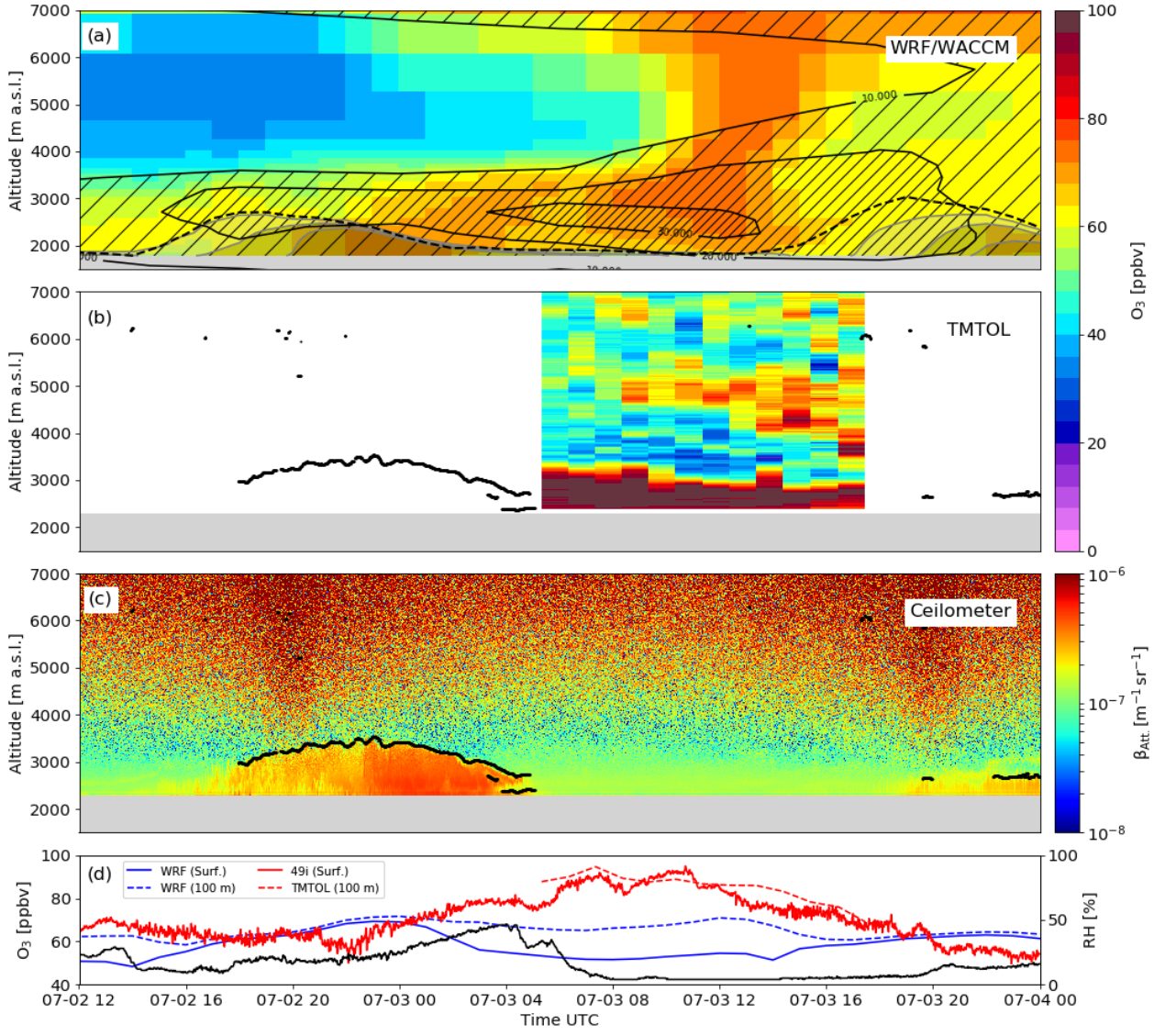

Figure 9. Overview of the model outputs and measurements over TMF between 2 July 12:00 and 4 July UTC. (a) WRF-Chem ozone mixing ratio over TMF (color scale), WRF-Chem anthropogenic CO (grey shaded contours), PBL height (dashed black) and WACCM stratospheric tracer (hatched contours). (b) TMTOL measurements (color scale) and PBL height (black points). The ozonesonde profile is shown overlaid at the time of the launch and surrounded by a black box. (c) Ceilometer-derived attenuated backscatter (color scale) and PBL height (black points). (d) WRF-Chem ozone mixing ratio at surface (solid blue) and 100 m a.g.l. (dashed blue) together with the 49i Ozone Analyzer surface ozone measurements (solid red), TMTOL ozone mixing ratio retrieval at 100 m a.g.l. (dashed red) and surface relative humidity (solid black).

https://doi.org/10.5194/acp-2020-1208
Preprint. Discussion started: 16 December 2020

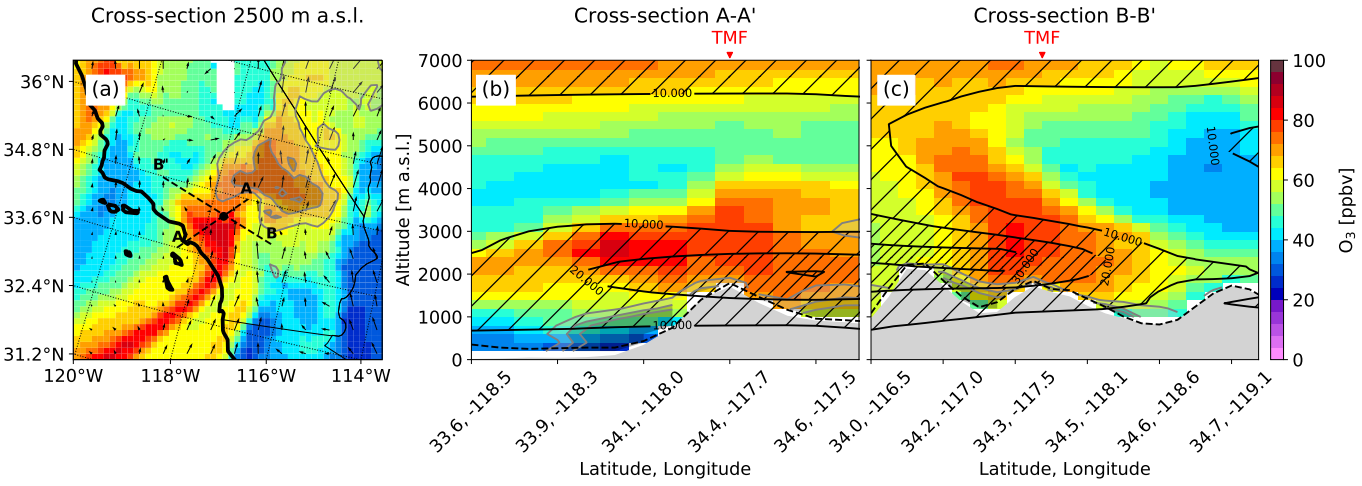

Figure 10. Horizontal and vertical cross-sections of WRF-Chem and WACCM forecast outputs for 3 July 6:00 UTC. (a) Horizontal cross-section at 2.5 km a.s.l. (b) Vertical cross-section along A-A' line. (c) Vertical cross-section along B-B' line. Total forecasted WRF-Chem ozone concentration is shown in a color scale (all panels). WRF-Chem anthropogenic CO levels (grey-shaded contours, all panels), WACCM stratospheric ozone (hatched contours, (b) and (c)) and WRF-Chem winds (arrows, (a)) are also shown.

surface ozone levels were compatible with a surface ozone exceedance event, which triggered the second extended TMTOL run. Figure 11b presents an overview of these two measurement sections, as well as the profile captured by an ozonesonde launched on 28 May 1:22 UTC (Fig. 12, solid) and the ceilometer-derived PBL height (Fig. 11c). During the first measurement section conducted between 27 May 1:24 UTC and 7:30 UTC, homogeneous ozone levels of about 70 ppbv were observed in the PBL, while the free troposphere was characterized homogeneous levels of about 40 ppbv. While TMTOL measurements and WRF-Chem are in qualitative agreement, the observed high ozone levels extended later in the day than the forecasted ones, which is compatible with the general behavior presented in Sec. 3.1. The ceilometer backscatter measurements presented in Fig. 11c show a strong correlation with the TMTOL profiles, with high ozone in the PBL associated with high aerosol levels. In contrast to the previous case study, where large differences were observed between the measured and forecasted surface ozone levels, the first part of this case study revealed a good agreement in the peak ozone mixing ratio (Fig. 11d).

In the case of the second TMTOL measurement period, conducted between 27 May 16:30 and 28 May 6:30 UTC, the PBL ozone mixing ratio follows a similar spatio-temporal progression as in the previous measurement section, including a similar temporal displacement in the ozone maximum with respect to the model forecast, similar PBL height and comparable ozone levels in the PBL and free troposphere. Despite these similarities, there is an interesting feature that makes this case specially interesting for air quality forecasting. While the simulated surface ozone was expected to exceed the 70 ppbv EPA standard at the transition between 27 May and 28 May, and high ozone levels were measured by TMTOL above 300 m a.g.l., almost no surface impact has been measured associated with the LA pollution transport event (Fig. 10d).

https://doi.org/10.5194/acp-2020-1208
Preprint. Discussion started: 16 December 2020

Atmospheric Chemistry and Physics Discussions

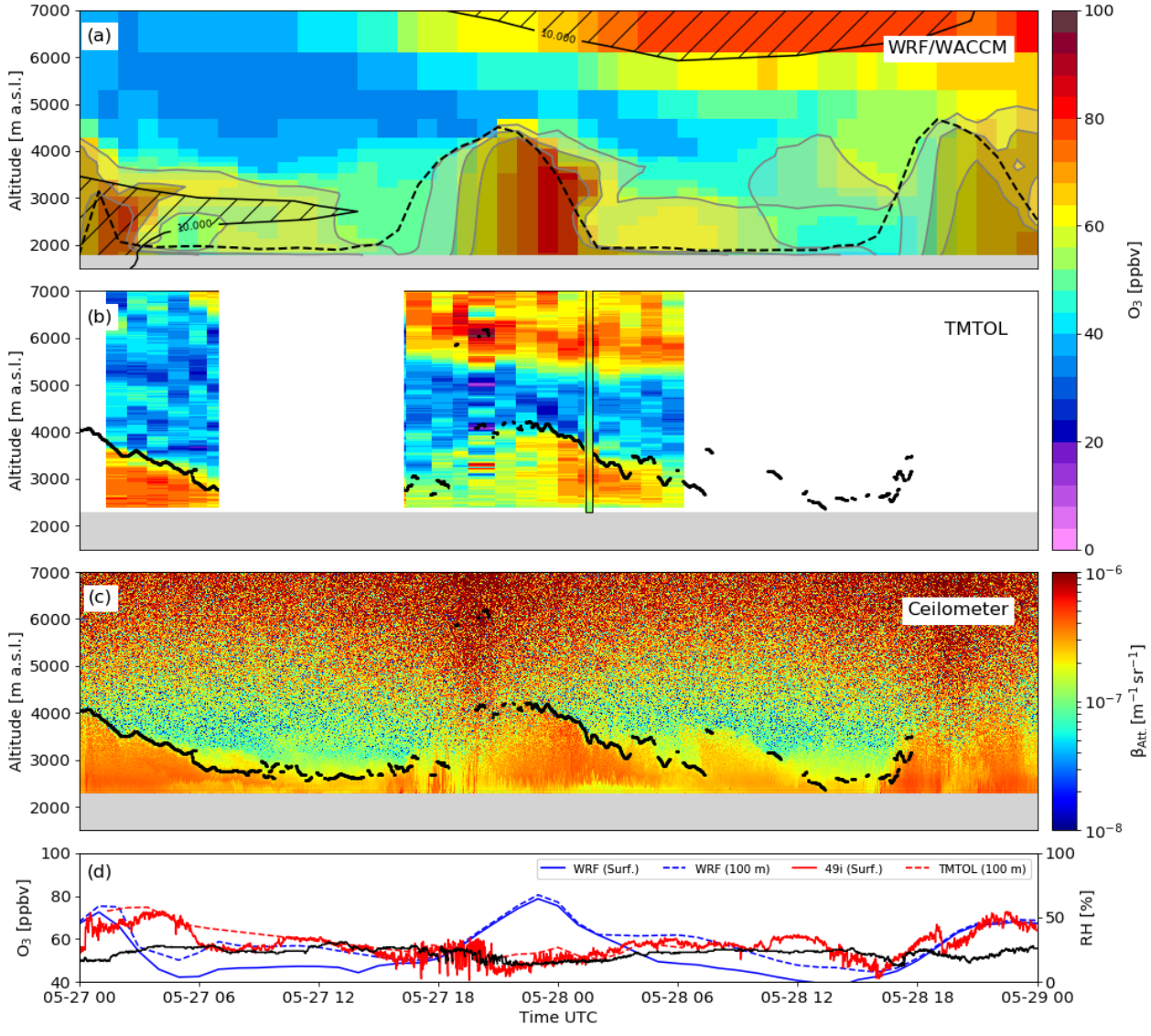

Figure 11. Overview of the model outputs and measurements over TMF between 27 May and 29 May UTC. Panel descriptions are the same as the ones shown for Fig. 9.

The origin of this discrepancy was traced back to two well-mixed near-ground layers bounded by very sharp temperature inversions (Fig. 12b) that prevented the ozone-laden air from LA from being down-mixed and affecting thus the surface ozone concentration. The inversions that bounded these two layers were found at 2480 m a.s.l. and 2660 m a.s.l.. The first layer, the closest one to the ground and about 200 m deep, was characterized by an ozone mixing ratio of about 55 ppbv and relative humidity of 20 %, while the second layer, about 150 m deep exhibited an ozone mixing ratio of about 65 ppbv and relative

https://doi.org/10.5194/acp-2020-1208
Preprint. Discussion started: 16 December 2020

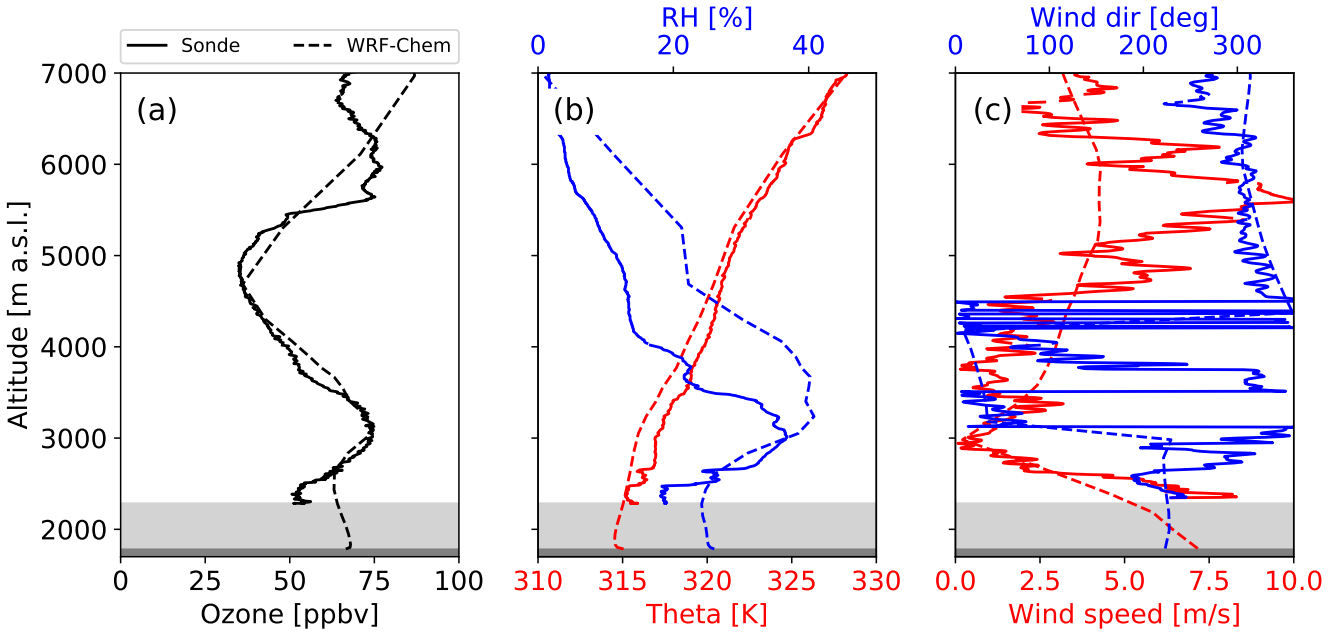

Figure 12. Sonde and corresponding WRF-Chem profiles for the launch conducted on 28 May 1:22 UTC. (a) Sonde ozone profile (solid black) and corresponding WRF-Chem output (dashed black). (b) Sonde-derived potential temperature (solid red) and relative humidity (solid blue) together with the corresponding WRF-Chem profiles (dashed, same colors). (c) Sonde-derived wind speed (solid red) and direction (solid blue) together with the corresponding WRF-Chem profiles (dashed, same colors). The actual TMF elevation (light grey shaded) is shown together with the model elevation (grey shaded).

humidity in the order of 27 %. Sitting on top of these two layers, we can see a 1.5 km deep layer characterized by relative high ozone mixing ratio (75 ppbv peak at 3 km a.s.l.) and a higher relative humidity that the other two layers (37 % at 3 km a.s.l.). The ceilometer profiles capture during the second TMTOL experiment shown in Fig. 10d exhibit a similar structure, with a relatively aerosol-poor layer below 2660 m a.s.l. and an aerosol-laden layer for the rest of the PBL. Finally, the wind profile presented in Fig. 12c revealed high north-westerly winds at low levels, which rapidly slow down and turn to northerly direction above 2660 m a.s.l.. While WRF-Chem forecast (Fig. 12, dashed) was able to forecast most of the previously mentioned features captured by the ozonesonde, including the undercutting of the LA basin pollution layer by an air mass characterized by lower ozone mixing ratio and lower humidity, the terrain smoothing caused this layer to have a limited impact on the surface, which translated into a large difference with regard to the forecasted surface ozone.

As in the previous case study, Fig. 13 provides a general overview of the WRF-Chem output for the LA basin and surrounding areas at the closes time from the ozonesonde profile (28 May 1:00 UTC). The 2500 m horizontal cross-section presented in Fig. 13a reveals a fairly large plume of LA pollution, characterized by high ozone and high anthropogenic CO, being transported eastwards. The A-A' cross-section shows an example of the typical mountain venting (or mountain chimney) effect, which has

https://doi.org/10.5194/acp-2020-1208
Preprint. Discussion started: 16 December 2020

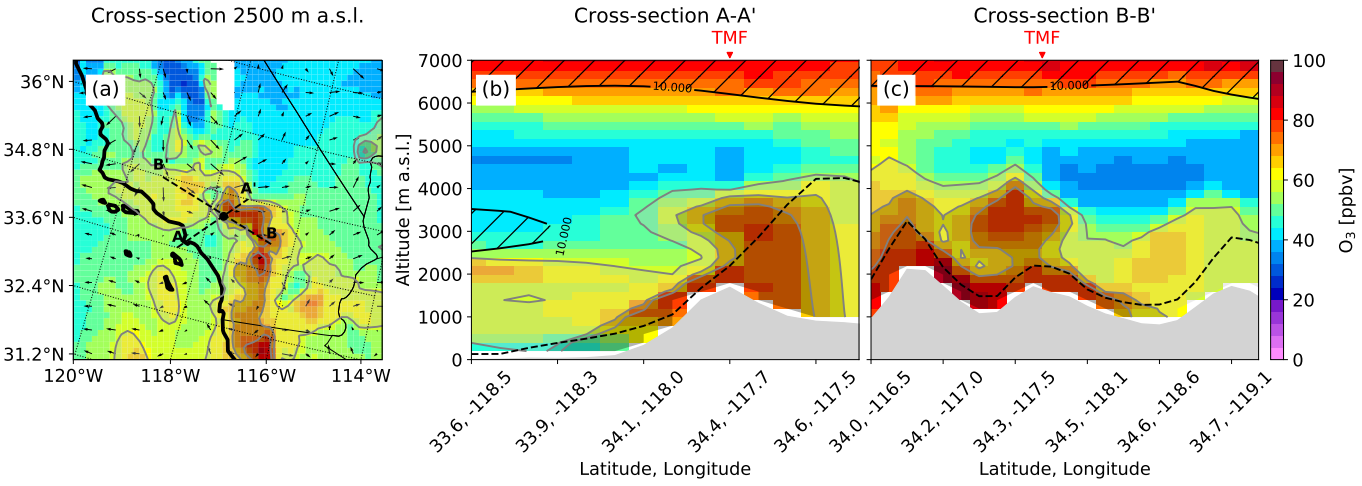

Figure 13. Horizontal and vertical cross-sections of WRF-Chem and WACCM forecast outputs for 28 May 1:00 UTC. Panel descriptions are the same as the ones shown for Fig. 10.

been previously identified as the main mechanism by which LA basin pollution is transported over the San Gabriel mountains and into the free troposphere (Langford et al., 2010). About 2.5 km a.s.l., a slight decrease in the ozone mixing ratio is visible over TMF on both cross-sections, which corresponds to the same undercutting dry and ozone-poor layer previously discussed.

4.3 11-15 June 2020: A combined case

In this case study, an extended TMTOL run conducted between 10 June 15:20 and 15 June 7:10 UTC is analyzed and compared to the WACCM and WRF-Chem forecasts. In contrast to the previous two case studies, this measurement period provides a more comprehensive and complex picture of the multi-day evolution of the different processes affecting the surface ozone levels at TMF.

During the first two days of this case study, the WRF-Chem and WACCM simulations (Fig. 14a) forecasted little stratospheric influence as well as considerable transport of LA basin pollution during 11 June. TMTOL ozone retrievals (Fig. 14b) and the ceilometer-derived PBL height (Fig. 14b, black) show very good qualitative agreement with the WRF-Chem simulations during 11 June, with larger differences observed during 12 June. During 11 June, a deep PBL reaching 4.5 km a.s.l. (11 June 0:00 UTC) can be inferred from both the forecast and the observations (TMTOL and Ceilometer), with enhanced ozone, anthropogenic CO and aerosol load. In the case of the WRF-Chem simulation, the ozone mixing ratio associated with this transport event was in the order of 70 ppbv at 100 m a.g.l. (Fig. 14d), which agreed well with TMTOL observations. Nevertheless, the simulations also show a very strong gradient in the lower 100 m, which resulted in an underestimation of the impact of this LA basin plume at the surface and prevented the forecasting of the exceedance as it finally happened. In the case of the 12 June forecast, the differences with the TMTOL, ceilometer, and surface instruments were larger compared to the previous day. WRF-Chem simulations forecasted only mild ozone transport, while TMTOL and the ceilometer measurements show ozone mixing ratios

https://doi.org/10.5194/acp-2020-1208
Preprint. Discussion started: 16 December 2020

Atmospheric Chemistry and Physics Discussions

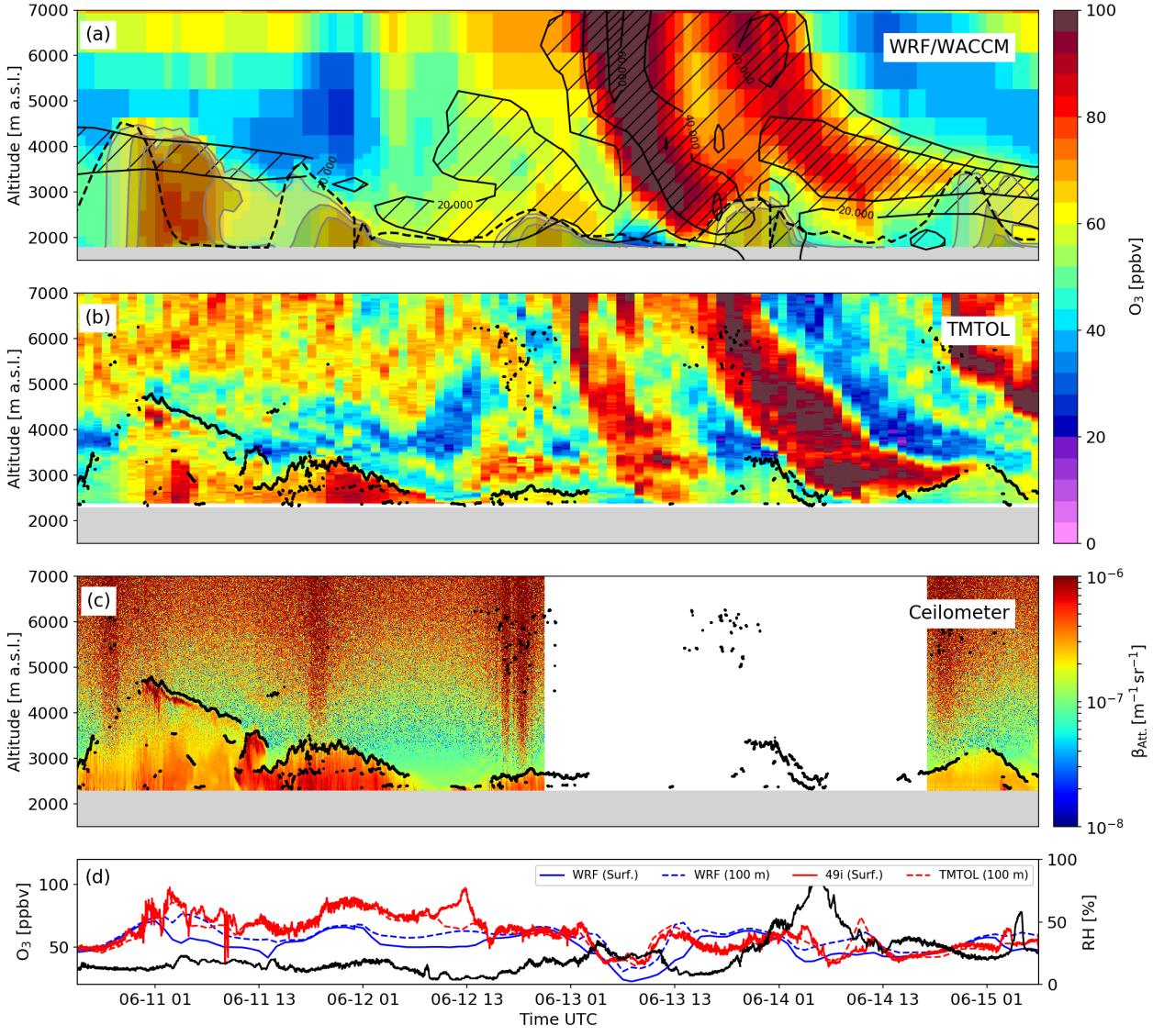

Figure 14. Overview of the model outputs and measurements over TMF between 10 June 15:20 and 15 June 7:10 UTC. Panel descriptions are the same as the ones shown for Fig. 9.

over 80 ppbv associated with a strong aerosol load. As in the previous day, the surface ozone records show a second exceedance, while the forecast underestimated the surface impact by about 20 ppbv. A remarkable feature can be seen on 12 June 13:00 UTC, when the irruption of a thin near-ground layer with high aerosol content made the surface ozone measurements climb briefly up to little under 100 ppbv, while keeping the 100 m a.g.l. TMTOL measurements unaffected.

https://doi.org/10.5194/acp-2020-1208
Preprint. Discussion started: 16 December 2020


Atmospheric Chemistry and Physics Discussions

Starting on 12 June 12:00 UTC, an increase in the stratospheric ozone contribution can be observed developing in WACCM and WRF-Chem forecasts above the PBL. This ozone enhancement, also visible in TMTOL profiles, is followed by two descending ozone-rich stratospheric air tongues. TMTOL observations indicate a good qualitative agreement of the model regarding these two deep intrusions, with some differences on their timing, spatial evolution, and ozone mixing ratio. Shortly after the first intrusion is seen appearing at 7 km a.s.l. (13 June 3:00 UTC), and coincident with the collapse of the PBL, a relatively sharp decrease in the surface ozone mixing ratio from 70 ppbv to 50 ppv can be seen in Fig. 14d. This decrease in the surface ozone concentration, associated with an increase in the relative humidity, resembles the case study presented in (Chouza et al., 2019) and suggest low-level transport of marine air as the source of it. By 13 June 13:00 UTC, the stratospheric intrusion reaches the surface over TMF, causing a decrease in the surface relative humidity and an increase in the surface ozone mixing ratio. The WRF-Chem ozone mixing ratio at 100 m a.g.l. shown in Fig. 14d shows a very good agreement with the TMTOL retrieval at that altitude, while the forecast of the surface ozone shows a considerable underestimation likely associated with the growth of the PBL and limited downward entrainment. In a similar way, the second intrusion is preceded by a decrease in the surface ozone and a strong increase of the relative humidity, associated with marine air transport (back-trajectories not shown). As the SI approaches the surface, the relative humidity decreases, and the surface ozone increases. While the near-ground TMTOL measurements (Fig. 14d) show an ozone mixing ratio peak of about 75 ppbv at the time the intrusion is at its minimum altitude over TMF, the surface ozone and the WRF forecast show only very weak signs of it. Finally, as the PBL starts to grow, the intrusion is pushed up generating a strong gradient between the PBL and the SI with no evident signs of ozone enhancement in the PBL due to entrainment neither in the model or the surface measurements.

5 Summary, conclusions and outlook

In the first part of this work, surface measurements conducted at TMF were used, in combination with WRF-Chem and WACCM simulations, to provide an overview of the near-surface ozone and PM10 characteristics at TMF. The results revealed a large number of days with ozone levels exceeding the National Ambient Air Quality Standards at TMF during late spring, summer and early fall, with the maximum during June. During this period, the surface influence of stratospheric intrusions is modeled to be at its minimum. This results, in combination with the large concentrations of anthropogenic CO forecasted by WRF-Chem at TMF, suggests that LA basin pollution plays a dominant role in these exceedance events. Backward-trajectories indicate that the surface ozone at TMF is highly sensitive to the wind regime, with the highest ozone typically observed associated with eastward transport from the Santa Clarita/San Fernando Valley area.

Making use of the enhanced spatial and temporal TMTOL measurements capabilities allowed by the recently installed very-near range channel and system automation, 726 vertical profiles of ozone measurements conducted during TROPOMI overpasses (noon) and shortly after sunset were used to conduct an evaluation of the ACOM WRF-Chem air-quality forecast over the period comprehended between May 2019 and September 2020. The comparison revealed a fairly good agreement in the PBL, with an altitude-increasing high-ozone positive bias reaching about 75% at 15 km a.s.l.. This bias appears to be season and time-independent. Additionally, three case studies showing stratospheric and LA basin driven exceedances were

https://doi.org/10.5194/acp-2020-1208
Preprint. Discussion started: 16 December 2020


Atmospheric Chemistry and Physics Discussions

discussed in light of the WRF-Chem and WACCM stratospheric forecast. A good agreement was observed between TMTOL measurements and simulations concerning the different mechanisms driving near-surface ozone, including LA basin transport through mountain slope effect and stratospheric intrusions.

While the results shown in this work point to the mountain chimney effect and associated LA basin transport as the main mechanism controlling the abundance of ozone and other pollutants in the PBL, residual layers, and lowermost troposphere over TMF, additional datasets including surface measurements of CO, NO_2 and stratospheric tracers (like beryllium-7) would provide additional support to this conclusion and allow a quantification of the actual stratospheric contribution to enhanced ozone levels. Additional lidar measurement capabilities, allowing simultaneous lidar measurements in the LA basin area, TMF, and Mojave desert would provide further evidence of regional transport as well as a better understanding of the impact of these elevated plumes on downwind ozone monitoring stations like those deployed in Mojave and Joshua Tree national parks. Furthermore, the deployment of such lidar systems in the Channel Islands, upwind from the LA basin, and where the impact of local sources is limited (Oltmans et al., 2008), would allow to better characterize and quantify the tropospheric ozone background conditions of air entering the west coast of the continental United States.

Data availability. The TMTOL data sets used in this study is publicly accessible at https://www-air.larc.nasa.gov/missions/TOLNet/data.html. ACOM WRF-Chem forecast output is accessible at https://www.acom.ucar.edu/firex-aq/FIREX-AQ/Evaluation/TOLNet/Wrightwood_CA/. ACOM WACCM dataset can be requested at https://www.acom.ucar.edu/waccm/download.shtml. For auxiliary datasets, please contact the authors.

Author contributions. Fernando Chouza prepared most of the manuscript and the statistical comparison with the rest of the datasets. Thierry Leblanc is the principal investigator of TMTOL and provided support in analysis of the TMTOL data. Gabriele Pfister, Rajesh Kumar and Carl Drews provided the WRF-Chem forecast used in this study. Simone Tilmes and Louisa Emmons provided the WACCM simulations used in this study. Mark Brewer and Patrick Wang provided technical support for the collection of the data included in this work. Sabino Piazzolla provided the ceilometer and PM10 data. All co-authors provided feedback on the manuscript.

Competing interests. The authors declare that they have no conflict of interest.

Acknowledgements. The research was carried out at the Jet Propulsion Laboratory, California Institute of Technology under a contract with the National Aeronautics and Space Administration (80NM0018D004). The development of the WRF-Chem forecasting system was supported by the NASA grant 80NSSC18K0681. We would like to acknowledge high-performance computing support from Cheyenne (doi:10.5065/D6RX99HX) provided by NCAR's Computational and Information Systems Laboratory, sponsored by the National Science Foundation. We acknowledge the use of the WRF-Chem preprocessor tool anthro_emis provided by the Atmospheric Chemistry Observa-

https://doi.org/10.5194/acp-2020-1208
Preprint. Discussion started: 16 December 2020

Atmospheric Chemistry and Physics Discussions

tions and Modeling Laboratory (ACOM) of NCAR. The National Center for Atmospheric Research is sponsored by the National Science
445 Foundation.

https://doi.org/10.5194/acp-2020-1208
Preprint. Discussion started: 16 December 2020

Atmospheric Chemistry and Physics Discussions

References

Brattich, E., Bracci, A., Zappi, A., Morozzi, P., Di Sabatino, S., Porcù, F., Di Nicola, F., and Tositti, L.: How to Get the Best from Low-Cost Particulate Matter Sensors: Guidelines and Practical Recommendations, Sensors, 20, 3073, https://doi.org/10.3390/s20113073, 2020.

Chen, C. M., Cageao, R. P., Lawrence, L., Stutz, J., Salawitch, R. J., Jourdain, L., Li, Q., and Sander, S. P.: Diurnal variation of midlatitudinal NO_3 column abundance over table mountain facility, California, Atmospheric Chemistry and Physics, 11, 963–978, https://doi.org/10.5194/acp-11-963-2011, 2011.

Chouza, F., Leblanc, T., Brewer, M., and Wang, P.: Upgrade and automation of the JPL Table Mountain Facility tropospheric ozone lidar (TMTOL) for near-ground ozone profiling and satellite validation, Atmos. Meas. Tech., 12, 569–583, https://doi.org/10.5194/amt-12-569-2019, 2019.

De Wekker, S. F. J. and Kossmann, M.: Convective Boundary Layer Heights Over Mountainous Terrain—A Review of Concepts, Front. Earth Sci., 3, 77, https://doi.org/10.3389/feart.2015.00077, 2015.

Emmons, L. K., Walters, S., Hess, P. G., Lamarque, J.-F., Pfister, G. G., Fillmore, D., Granier, C., Guenther, A., Kinnison, D., Laepple, T., Orlando, J., Tie, X., Tyndall, G., Wiedinmyer, C., Baughcum, S. L., and Kloster, S.: Description and evaluation of the Model for Ozone and Related chemical Tracers, version 4 (MOZART-4), Geosci. Model Dev., 3, 43–67, https://doi.org/10.5194/gmd-3-43-2010, 2010.

Emmons, L. K., Schwantes, R. H., Orlando, J. J., Tyndall, G., Kinnison, D., Lamarque, J.-F., Marsh, D., Mills, M. J., Tilmes, S., Bardeen, C., Buchholz, R. R., Conley, A., Gettelman, A., Garcia, R., Simpson, I., Blake, D. R., Meinardi, S., and Pétron, G.: The Chemistry Mechanism in the Community Earth System Model Version 2 (CESM2), J. Adv. Model. Earth Syst., 12, e2019MS001 882, https://doi.org/10.1029/2019MS001882, 2020.

EPA: Nonattainment Areas for Criteria Pollutants (Green Book), https://www.epa.gov/green-book, 2020.

Fast, J. D., Gustafson Jr, W. I., Easter, R. C., Zaveri, R. A., Barnard, J. C., Chapman, E. G., Grell, G. A., and Peckham, S. E.: Evolution of ozone, particulates, and aerosol direct radiative forcing in the vicinity of Houston using a fully coupled meteorology-chemistry-aerosol model, J. Geophys. Res. D: Atmos., 111, https://doi.org/10.1029/2005JD006721, 2006.

Freitas, S. R., Longo, K. M., Chatfield, R., Latham, D., Silva Dias, M. A. F., Andreae, M. O., Prins, E., Santos, J. C., Gielow, R., and Carvalho Jr., J. A.: Including the sub-grid scale plume rise of vegetation fires in low resolution atmospheric transport models, Atmos. Chem. Phys., 7, 3385–3398, https://doi.org/10.5194/acp-7-3385-2007, 2007.

Gettelman, A., Mills, M. J., Kinnison, D. E., Garcia, R. R., Smith, A. K., Marsh, D. R., Tilmes, S., Vitt, F., Bardeen, C. G., McInerny, J., Liu, H.-L., Solomon, S. C., Polvani, L. M., Emmons, L. K., Lamarque, J.-F., Richter, J. H., Glanville, A. S., Bacmeister, J. T., Phillips, A. S., Neale, R. B., Simpson, I. R., DuVivier, A. K., Hodzic, A., and Randel, W. J.: The Whole Atmosphere Community Climate Model Version 6 (WACCM6), J. Geophys. Res. D: Atmos., 124, 12 380–12 403, https://doi.org/10.1029/2019JD030943, 2019.

Gorham, K. A., Blake, N. J., VanCuren, R. A., Fuelberg, H. E., Meinardi, S., and Blake, D. R.: Seasonal and diurnal measurements of carbon monoxide and nonmethane hydrocarbons at Mt. Wilson, California: Indirect evidence of atomic Cl in the Los Angeles basin, Atmos. Environ., 44, 2271–2279, https://doi.org/https://doi.org/10.1016/j.atmosenv.2010.04.019, 2010.

Granados-Muñoz, M. J. and Leblanc, T.: Tropospheric ozone seasonal and long-term variability as seen by lidar and surface measurements at the JPL-Table Mountain Facility, California, Atmos. Chem. Phys., 16, 9299–9319, https://doi.org/10.5194/acp-16-9299-2016, 2016.

Grell, G. A., Peckham, S. E., Schmitz, R., McKeen, S. A., Frost, G., Skamarock, W. C., and Eder, B.: Fully coupled "online" chemistry within the WRF model, Atmos. Environ., 39, 6957–6975, https://doi.org/10.1016/j.atmosenv.2005.04.027, 2005.

https://doi.org/10.5194/acp-2020-1208
Preprint. Discussion started: 16 December 2020

Guenther, A. B., Jiang, X., Heald, C. L., Sakulyanontvittaya, T., Duhl, T., Emmons, L. K., and Wang, X.: The Model of Emissions of Gases and Aerosols from Nature version 2.1 (MEGAN2.1): an extended and updated framework for modeling biogenic emissions, Geosci. Model Dev., 5, 1471–1492, https://doi.org/10.5194/gmd-5-1471-2012, 2012.

Knowland, K. E., Ott, L. E., Duncan, B. N., and Wargan, K.: Stratospheric Intrusion-Influenced Ozone Air Quality Exceedances Investigated in the NASA MERRA-2 Reanalysis, Geophys. Res. Lett., 44, 10,691–10,701, https://doi.org/10.1002/2017GL074532, 2017.

Langford, A., Alvarez, R., Brioude, J., Evan, S., Iraci, L., Kirgis, G., Kuang, S., Leblanc, T., Newchurch, M., Pierce, R., Senff, C., and Yates, E.: Coordinated profiling of stratospheric intrusions and transported pollution by the Tropospheric Ozone Lidar Network (TOLNet) and NASA Alpha Jet experiment (AJAX): Observations and comparison to HYSPLIT, RAQMS, and FLEXPART, Atmos. Environ., 174, 1–14, https://doi.org/10.1016/j.atmosenv.2017.11.031, 2018.

Langford, A. O., Senff, C. J., Alvarez II, R. J., Banta, R. M., and Hardesty, R. M.: Long-range transport of ozone from the Los Angeles Basin: A case study, Geophys. Res. Lett., 37, https://doi.org/10.1029/2010GL042507, 2010.

Leblanc, T., Sica, R. J., Van Gijsel, J. A., Godin-Beekmann, S., Haefele, A., Trickl, T., Payen, G., and Gabarrot, F.: Proposed standardized definitions for vertical resolution and uncertainty in the NDACC lidar ozone and temperature algorithms–Part 1: Vertical resolution, Atmos. Meas. Tech., 9, 4029–4049, 2016.

Leblanc, T., Brewer, M. A., Wang, P. S., Granados-Muñoz, M. J., Strawbridge, K. B., Travis, M., Firanski, B., Sullivan, J. T., McGee, T. J., Sumnicht, G. K., Twigg, L. W., Berkoff, T. A., Carrion, W., Gronoff, G., Aknan, A., Chen, G., Alvarez, R. J., Langford, A. O., Senff, C. J., Kirgis, G., Johnson, M. S., Kuang, S., and Newchurch, M. J.: Validation of the TOLNet lidars: the Southern California Ozone Observation Project (SCOOP), Atmos. Meas. Tech., 11, 6137–6162, https://doi.org/10.5194/amt-11-6137-2018, 2018.

Lee, T. R., Wekker, S. F. J. D., Pal, S., Andrews, A. E., and Kofler, J.: Meteorological controls on the diurnal variability of carbon monoxide mixing ratio at a mountaintop monitoring site in the Appalachian Mountains, Tellus B: Chem. Phys. Meteorol., 67, 25 659, https://doi.org/10.3402/tellusb.v67.25659, 2015.

Lin, M., Fiore, A. M., Cooper, O. R., Horowitz, L. W., Langford, A. O., Levy II, H., Johnson, B. J., Naik, V., Oltmans, S. J., and Senff, C. J.: Springtime high surface ozone events over the western United States: Quantifying the role of stratospheric intrusions, J. Geophys. Res. D: Atmos., 117, https://doi.org/10.1029/2012JD018151, 2012a.

Lin, M., Fiore, A. M., Horowitz, L. W., Cooper, O. R., Naik, V., Holloway, J., Johnson, B. J., Middlebrook, A. M., Oltmans, S. J., Pollack, I. B., Ryerson, T. B., Warner, J. X., Wiedinmyer, C., Wilson, J., and Wyman, B.: Transport of Asian ozone pollution into surface air over the western United States in spring, J. Geophys. Res. D: Atmos., 117, https://doi.org/10.1029/2011JD016961, 2012b.

Lin, M., Horowitz, L. W., Payton, R., Fiore, A. M., and Tonnesen, G.: US surface ozone trends and extremes from 1980 to 2014: quantifying the roles of rising Asian emissions, domestic controls, wildfires, and climate, Atmos. Chem. Phys., 17, 2943–2970, https://doi.org/10.5194/acp-17-2943-2017, 2017.

Lu, R. and Turco, R. P.: Ozone distributions over the los angeles basin: Three-dimensional simulations with the smog model, Atmos. Environ., 30, 4155–4176, https://doi.org/10.1016/1352-2310(96)00153-7, 1996.

Mauzerall, D. L. and Wang, X.: Protecting agricultural crops from the effects of tropospheric ozone exposure: reconciling science and standard setting in the United States, Europe, and Asia, Annu. Rev. Energy Env., 26, 237–268, 2001.

McDermid, I. S., Haner, D. A., Kleiman, M. M., Walsh, T. D., and White, M. L.: Differential absorption lidar systems for tropospheric and stratospheric ozone measurements, Opt. Eng., 30, https://doi.org/10.1117/12.55768, 1991.

McDermid, I. S., Beyerle, G., Haner, D. A., and Leblanc, T.: Redesign and improved performance of the tropospheric ozone lidar at the Jet Propulsion Laboratory Table Mountain Facility, Appl. Opt., 41, 7550–7555, https://doi.org/10.1364/AO.41.007550, 2002.

https://doi.org/10.5194/acp-2020-1208
Preprint. Discussion started: 16 December 2020

Monks, P. S., Archibald, A. T., Colette, A., Cooper, O., Coyle, M., Derwent, R., Fowler, D., Granier, C., Law, K. S., Mills, G. E., Stevenson, D. S., Tarasova, O., Thouret, V., von Schneidemesser, E., Sommariva, R., Wild, O., and Williams, M. L.: Tropospheric ozone and its precursors from the urban to the global scale from air quality to short-lived climate forcer, Atmos. Chem. Phys., 15, 8889–8973, https://doi.org/10.5194/acp-15-8889-2015, 2015.

Münkel, C. and Roininen, R.: Investigation of boundary layer structures with ceilometer using a novel robust algorithm, Tech. rep., American Meteorological Society, 2010.

Oltmans, S. J., Lefohn, A. S., Harris, J. M., and Shadwick, D. S.: Background ozone levels of air entering the west coast of the US and assessment of longer-term changes, Atmos. Environ., 42, 6020–6038, 2008.

Pollack, I. B., Ryerson, T. B., Trainer, M., Neuman, J. A., Roberts, J. M., and Parrish, D. D.: Trends in ozone, its precursors, and related secondary oxidation products in Los Angeles, California: A synthesis of measurements from 1960 to 2010, J. Geophys. Res. D: Atmos., 118, 5893–5911, https://doi.org/10.1002/jgrd.50472, 2013.

Powers, J. G., Klemp, J. B., Skamarock, W. C., Davis, C. A., Dudhia, J., Gill, D. O., Coen, J. L., Gochis, D. J., Ahmadov, R., Peckham, S. E., Grell, G. A., Michalakes, J., Trahan, S., Benjamin, S. G., Alexander, C. R., Dimego, G. J., Wang, W., Schwartz, C. S., Romine, G. S., Liu, Z., Snyder, C., Chen, F., Barlage, M. J., Yu, W., and Duda, M. G.: The Weather Research and Forecasting Model: Overview, System Efforts, and Future Directions, Bull. Am. Meteorol. Soc., 98, 1717–1737, https://doi.org/10.1175/BAMS-D-15-00308.1, 2017.

Stein, A. F., Draxler, R. R., Rolph, G. D., Stunder, B. J. B., Cohen, M. D., and Ngan, F.: NOAA's HYSPLIT Atmospheric Transport and Dispersion Modeling System, Bull. Am. Meteorol. Soc., 96, 2059–2077, https://doi.org/10.1175/BAMS-D-14-00110.1, 2016.

Stohl, A., Spichtinger-Rakowsky, N., Bonasoni, P., Feldmann, H., Memmesheimer, M., Scheel, H., Trickl, T., Hübener, S., Ringer, W., and Mandl, M.: The influence of stratospheric intrusions on alpine ozone concentrations, Atmos. Environ., 34, 1323–1354, https://doi.org/10.1016/S1352-2310(99)00320-9, 2000.

Tilmes, S., Hodzic, A., Emmons, L. K., Mills, M. J., Gettelman, A., Kinnison, D. E., Park, M., Lamarque, J.-F., Vitt, F., Shrivastava, M., Campuzano-Jost, P., Jimenez, J. L., and Liu, X.: Climate Forcing and Trends of Organic Aerosols in the Community Earth System Model (CESM2), J. Adv. Model. Earth Syst., 11, 4323–4351, https://doi.org/10.1029/2019MS001827, 2019.

Tsamalis, C., Ravetta, F., Gheusi, F., Delbarre, H., and Augustin, P.: Mixing of free-tropospheric air with the lowland boundary layer during anabatic transport to a high altitude station, Atmos. Res., 143, 425–437, https://doi.org/10.1016/j.atmosres.2014.03.011, 2014.

VanCuren, R.: Transport aloft drives peak ozone in the Mojave Desert, Atmos. Environ., 109, 331–341, https://doi.org/10.1016/j.atmosenv.2014.09.057, 2015.

Warner, M. S.: Introduction to PySPLIT: a Python toolkit for NOAA ARL's HYSPLIT model, Comput. Sci. Eng., 20, 47–62, https://doi.org/10.1109/MCSE.2017.3301549, 2018.

WHO: Health aspects of air pollution with particulate matter, ozone and nitrogen dioxide: report on a WHO working group, Bonn, Germany 13-15 January 2003, 2003.

Wiedinmyer, C., Akagi, S. K., Yokelson, R. J., Emmons, L. K., Al-Saadi, J. A., Orlando, J. J., and Soja, A. J.: The Fire INventory from NCAR (FINN): a high resolution global model to estimate the emissions from open burning, Geosci. Model Dev., 4, 625–641, https://doi.org/10.5194/gmd-4-625-2011, 2011.

Wiegner, M., Madonna, F., Binietoglou, I., Forkel, R., Gasteiger, J., Geiß, A., Pappalardo, G., Schäfer, K., and Thomas, W.: What is the benefit of ceilometers for aerosol remote sensing? An answer from EARLINET, Atmos. Meas. Tech., 7, 1979–1997, https://doi.org/10.5194/amt-7-1979-2014, 2014.